Radiology

ORIGINAL RESEARCH • EVIDENCE-BASED PRACTICE

Prevalence and Incidence of Paramagnetic Rim Lesions in Multiple Sclerosis: A Systematic Review and Meta-Analysis

Mario Tranfa, MD[1,2] • *Valeria Cantoni, PhD*[1] • *Roberta Green, PhD*[1] • *Guglielmo Carignani, MD*[1] • *Serena Capasso, MD*[1] • *Vincenzo Brescia Morra, MD*[3] • *Antonio Carotenuto, MD, PhD*[3] • *Alberto Cuocolo, MD*[1] • *Roberta Lanzillo, MD, PhD*[3] • *Marcello Moccia, MD, PhD*[4,5] • *Arnaldo Stanzione, MD, PhD*[1] • *Margherita Tarantino, MD*[1] • *Fabio Tortora, MD, PhD*[1] • *Giuseppe Pontillo, MD, PhD*[1,2,6,7] • *Sirio Cocozza, MD, PhD*[1] • *Maria Petracca, MD, PhD*[8]

Author affiliations, funding, and conflicts of interest are listed at the end of this article.

Radiology 2025; 316(3):e243718 • https://doi.org/10.1148/radiol.243718 • Content codes: NR MR

Background: Paramagnetic rim lesions (PRLs) hold implications for diagnosis and prognosis of multiple sclerosis (MS). However, the factors influencing their identification have yet to be fully clarified.

Purpose: To conduct a systematic review and meta-analysis assessing clinical and imaging-related factors affecting PRL identification, incidence, prevalence, evolution over time, and topography in patients with MS.

Materials and Methods: An English literature search was performed using PubMed and Embase databases to identify eligible studies published by February 8, 2024, with no restrictions on the earliest publication date. Risk of bias was assessed with a customized 12-item checklist. Meta-analyses of proportions were used to derive PRL-pooled prevalence, incidence, and CIs, at both the lesion and patient levels. Heterogeneity was assessed using the Cochran Q test and I^2 statistic. Sources of heterogeneity were explored via subgroup analyses and meta-regression analyses.

Results: Fifty-eight studies investigating 4532 patients with MS (mean age, 39 years ± 1.1 [SD]) were included. PRL prevalence was 0.12 (95% CI: 0.09, 0.16; 32 studies) at the lesion level and 0.52 (95% CI: 0.47, 0.58; 37 studies) at the patient level. Incidence was 0.23 (95% CI: 0, 0.75; three studies) at the lesion level and 0.11 (95% CI: 0, 0.47; two studies) at the patient level. No difference was observed for the lesion-level prevalence according to the PRL definition used ($P = .66$) or brain compartment ($P = .34$), and for the patient-level prevalence according to age ($P = .29$), disease duration ($P = .72$), or MS phenotype ($P = .29$). A subgroup analysis revealed differences in lesion-level prevalence based on lesion stage, field strength, MRI sequence, and resolution ($P < .001$ for all). The heterogeneity in prevalence across studies was high on average ($I^2 = 88.8\%$ and 99.2% at patient-wise and lesion-wise level, respectively). In 21% (12 of 58) of the studies, a clear definition of PRLs was not provided.

Conclusion: Although PRLs could be identified in approximately half of patients with MS undergoing imaging, the incidence of new PRLs was relatively low, and PRL prevalence was heterogeneous across studies.

Supplemental material is available for this article.

Multiple sclerosis (MS) is a chronic immune-mediated disease of the central nervous system with rising prevalence worldwide (1) and high personal and social costs (2,3). Early diagnosis and timely therapeutic intervention are crucial to mitigate the disease impact. The use of MRI in the diagnostic work-up has significantly improved diagnostic sensitivity (4). In recent years, emerging MRI biomarkers such as paramagnetic rim lesions (PRLs) and central vein sign (4) have been proposed to enhance diagnostic specificity and limit the misdiagnosis rate, which is estimated to range from 5% to 18% in contemporary cohorts (5). Indeed, the latest revision of the McDonald criteria (6) has introduced central vein sign and PRLs as optional diagnostic tools. In particular, the presence of at least one PRL has shown high specificity in distinguishing MS from mimics and healthy controls (7). Beyond their role in MS diagnosis, PRLs seem to hold prognostic significance and could represent a novel therapeutic target. PRLs may expand over time, show limited or absent remyelination (8), and are associated with a more severe clinical outcome, independent of age and disease duration (9).

Histologically, PRLs reflect MS-specific pathologic features, with an inactive demyelinated center, surrounded by iron-laden activated macrophages and microglia (10). At MRI, PRLs are T2 hyperintense, do not enhance with gadolinium-based contrast agents, and are characterized by a partial or complete paramagnetic rim (11).

Conflicting results have emerged regarding the epidemiology of PRLs, with high variability in reported prevalence rates of the overall lesion load (ranging from 2.3% to 41.0%) (12,13), their presence across patients (from 6.7% to 90.0%), and their topographic distribution (7,14,15). Clinical factors (relapsing or progressive phenotype, age, disease duration) and technical and/or methodological factors (MRI field strength, imaging sequence and postprocessing technique, spatial resolution) have been suggested as relevant contributors to such discrepancies (11,16–18). A previous systematic review by Kwong and colleagues (18), based on 1230 patients and 29 studies, addressed the topic of PRL prevalence. However, it assessed only a subset of the potential biologic and methodologic factors influencing PRL detection. Moreover, since the publication of that review, several studies have further focused on PRLs, attesting to the growing interest of the scientific community and the efforts toward the clinical translation of this biomarker.

The aim of this systematic review and meta-analysis was to assess clinical and imaging-related factors affecting PRL identification, as well as PRL incidence, prevalence, evolution over time, and topography in patients with MS.

Abbreviations

MS = multiple sclerosis, NAIMS = North American Imaging in Multiple Sclerosis, PRL = paramagnetic rim lesion

Summary

Although paramagnetic rim lesions (PRLs) could be identified in approximately half of patients with multiple sclerosis undergoing imaging, the incidence of new PRLs was relatively low and PRL prevalence was heterogeneous across studies.

Key Results

- In this systematic review and meta-analysis of 58 studies investigating 4532 patients with multiple sclerosis, the patient-level pooled prevalence of paramagnetic rim lesions (PRLs) was 0.52 (95% CI: 0.47, 0.58), and the incidence of new PRLs over a mean follow-up of 4.7 years was 0.11 (95% CI: 0, 0.47).
- Subgroup analysis revealed differences in lesion-level PRL prevalence based on field strength, MRI sequence, image resolution, and lesion stage ($P < .001$ for all).
- PRL prevalence across studies was highly heterogeneous (I^2 of 88.8% and 99.2% at patient-wise and lesion-wise level, respectively), and there was a lack of a clear definition for PRLs in 21% (12 of 58) of studies.

Materials and Methods

This meta-analysis follows the Preferred Reporting Items for Systematic Reviews and Meta-Analyses (PRISMA) statement (PRISMA Checklist in Appendix S1) (19). The study is registered with the international Prospective Register of Systematic Reviews (PROSPERO; ID no. CRD42024525858). Ethical approval was not needed.

Data Sources and Search Strategy

An English literature search was performed using the PubMed and Embase databases to identify articles published by February 8, 2024, with no restrictions on the earliest publication date. Controlled vocabulary, including Medical Subject Heading (or MeSH) terms with all subheadings, supplemented with keywords (ie, "chronic active lesion," "rim lesion," "iron rim," "smoldering lesion," "MRI," "PET," "multiple sclerosis"), was used to conduct the search. See Appendix S1 for the full search strategy.

The title and abstract of potentially relevant studies were screened for appropriateness (by G.C. and M.P.). Disagreements were resolved by consensus. Publications were included if they met the following criteria: *(a)* patients exhibited radiologically isolated syndrome, clinically isolated syndrome, or MS; *(b)* the brain MRI protocol included susceptibility-weighted imaging, quantitative susceptibility mapping, fluid-attenuated inversion recovery*, R2*, or any other T2*-dependent modalities; *(c)* outcomes of interest included PRLs; and *(d)* they provided data allowing for the calculation of patient-level prevalence and/or lesion-level prevalence of PRLs. Studies were excluded if they were *(a)* review articles, qualitative studies, letters, editorials, opinions, or conference abstracts; *(b)* based on postmortem MRI; *(c)* animal studies; or *(d)* studies using sequences with partial supratentorial brain coverage. In cases of cohort overlap, the study with the largest sample size was selected (Fig 1). To clarify potential overlap between study cohorts described in different articles by the same groups, corresponding authors of each publication were directly contacted. When multiple MRI sequences or field strengths were available within the same study, quantitative susceptibility mapping data and data acquired at the highest field strength were retained, respectively, in line with previous studies demonstrating their greater specificity for PRL identification (18,20). Both prospective and retrospective studies were considered eligible. The full-published reports of the abstracts selected by the reviewers were retrieved, and the reviewers independently performed a second-step selection applying the inclusion and exclusion criteria; disagreements were resolved by consensus. The bibliographies of retrieved articles were manually reviewed for additional citations.

Data Extraction

Data extraction was performed (G.C.) and reviewed (M.P.). In case of disagreement, another author (S. Cocozza) was consulted to achieve consensus. The following information was retrieved

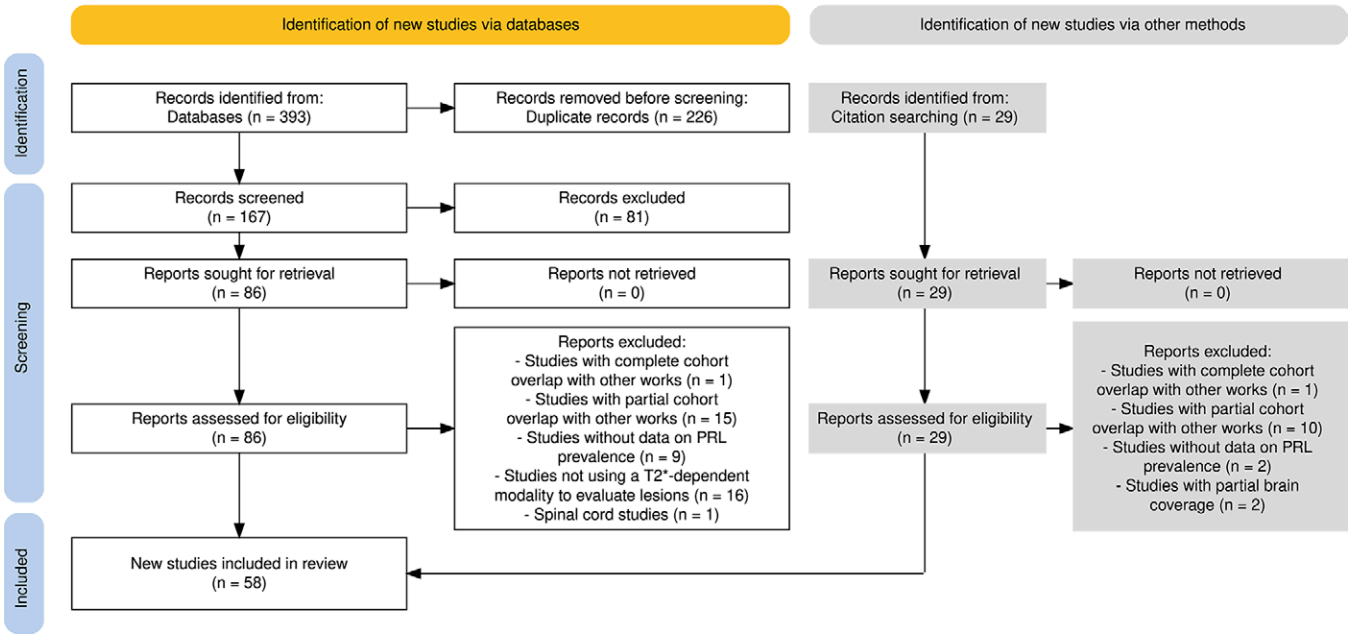

Figure 1: Diagram of literature search and selection process of studies included in analysis conducted between February and July 2024. PRL = paramagnetic rim lesion.

from each full-text article: *(a)* patient-level prevalence (proportion of patients with at least one PRL) and lesion-level prevalence (proportion of white matter lesions identified as PRLs) of PRLs; *(b)* bibliographic data; *(c)* study design; *(d)* imaging features; and *(e)* study population features.

Excluded publications and reasons for exclusion can be found in Table S1.

Quality Assessment

A 12-item checklist for risk of bias assessment was customized (M.P., V.C., and R.G.) to assess the quality of studies included in the meta-analysis, adapting items from the Joanna Briggs Institute Critical Appraisal Checklist for Prevalence Studies (21) and the National Institutes of Health Quality Assessment Tool for Observational Cohort and Cross-Sectional Studies *(https://www.nhlbi.nih.gov/health-topics/study-quality-assessment-tools)* (Appendix S1). Items were scored as low risk, moderate risk, and high risk. Two researchers (S. Capasso, M. Tranfa) independently assessed the risk of bias, and any disagreement was resolved by discussion.

Statistical Analysis

A systematic analytic approach was used to compute the pooled patient-level and lesion-level prevalence of PRLs from all eligible studies. Meta esize in Stata (StataCorp) was used to perform meta-analyses of proportions to derive pooled estimates, allowing evaluation of exact binomial and test score–based CIs. This procedure offers appropriate strategies for handling proportions close to the margins by use of the binomial distribution to model the within-study variability, or by allowing Freeman-Tukey double arcsine transformation to stabilize the variances. A random effects model was selected to summarize the prevalence of PRLs using proportions and 95% CIs. Heterogeneity was assessed using the Cochran Q test and the I^2 statistic. An I^2 greater than 50% was considered to represent substantial heterogeneity.

Incidence rates of PRLs were also calculated for each study with available data, and the pooled incidence rate of PRLs was estimated using the aforementioned random effects model. Sources of heterogeneity were explored via subgroup and meta-regression analyses. Subgroup analyses were conducted according to different field strengths (3 T, 4 T, 7 T), MRI sequences (susceptibility-weighted imaging, quantitative susceptibility mapping, T2*-weighted imaging), MRI resolutions (two-dimensional: submillimeter in-plane and ≤3 mm through-plane resolution; three-dimensional: ≤2 mm or higher resolution isotropic; other), PRL definitions (definition adherent to North American Imaging in Multiple Sclerosis [NAIMS] recommendations [22], definition not adherent to NAIMS recommendations), brain compartment (supratentorial, whole brain), lesion stage (acute, chronic), and MS phenotype (radiologically isolated syndrome, clinically isolated syndrome, relapsing-remitting MS, progressive MS, only when individual prevalences were reported in the text). Meta-regression analysis was performed to assess whether study-level variables, such as age and disease duration, were associated with the pooled patient-level prevalence of PRLs. Meta-regression is used to investigate whether between-study heterogeneity can be explained by one or more moderators. *P* values for the subgroup and meta-regression analyses were corrected for multiple comparisons using the Benjamini-Hochberg procedure and considered significant when $P < .05$. For post hoc comparisons, *P* value correction was performed with the Bonferroni procedure. Therefore, all *P* values reported in the Results section are adjusted for multiple comparisons. All statistical analyses and graphics were conducted using Stata version 18.0 (StataCorp) (V.C. and R.G.).

Results

Search Results and Study Characteristics

Results of the literature review and study selection are presented in Figure 1. The initial search identified 393 potentially eligible citations. Additionally, 29 full-text articles were obtained through handsearching reference lists of eligible studies or relevant articles. After removing 226 duplicates, 196 records were screened based on titles and abstracts. Subsequently, 81 citations were discharged according to inclusion and/or exclusion criteria (40 nonoriginal research articles, 20 conference abstracts, 18 postmortem or animal studies, three studies in languages other than English). Thus, 115 full-text articles were assessed for eligibility. After revision, 57 articles were excluded (16 for not using a T2*-dependent modality to evaluate lesions, 11 for not providing data useful for prevalence calculation, one for focusing on the spinal cord, two with partial supratentorial brain coverage, and 27 due to cohort overlaps).

Fifty-eight studies investigating 4532 patients with MS (mean age, 39 years ± 1.1 [SD]; range, 14.7–48.8 years; 2978 women, 1436 men, and 118 not specified) were included (Table 1). Examples of PRLs identified by different methodological and technical factors are shown in Figure 2.

Most studies surviving the selection process presented cross-sectional data ($n = 47$), whereas 11 studies presented both cross-sectional and longitudinal data. Among the 58 studies, three PET studies (of which one reported PRL prevalence from both PET and 3-T MRI) and three studies enrolling patients with pediatric-onset MS were identified. The field strength adopted across MRI studies ranged from 1.5 T to 7 T (3 T = 39 studies; 7 T = 14 studies; 1.5, 3, and 4 T = one study; 1.5 or 3 T = one study; 1.5 T = one study). Sequences for PRL identification included susceptibility-weighted imaging (24 studies), T2*-weighted imaging (15 studies), quantitative susceptibility mapping (15 studies), and other (one study). One study employed two sequences (T2*-weighted, quantitative susceptibility mapping).

For image resolution, 30 studies employed a two-dimensional sequence, whereas 15 studies employed a three-dimensional sequence. Six studies used sequences outside the aforementioned definitions, four lacked image resolution details, and one study used different resolutions for different field strengths. Among MRI studies with a cross-sectional component, three focused on acute PRLs (lesions that enhanced with gadolinium-based contrast agent administration), 24 focused on chronic PRLs (lesions that did not enhance with gadolinium-based contrast material), and one considered both acute and chronic PRLs in separate analyses; 28 studies did not differentiate between acute and chronic PRLs. Only three studies adhered to NAIMS recommendations to define PRLs. Sixteen studies focused on the supratentorial compartment and 14 conducted a whole-brain analysis; the remaining studies did not provide this information. Studies on acute PRLs were considered separately. Results of PET studies are reported descriptively.

Table 1: Study Characteristics

Study and Year	Institution	SC or MC	Enrollment Dates	Study Design	Method	MRI Sequence	Field Strength	Resolution	PRL Definition with NAIMS	Brain Compartment	Lesion Stage Considered
Absinta et al, 2019 (9)	National Institutes of Health (USA)	SC	January 1, 2012, to March 30, 2018	CS	MRI	T2*w	7 T	2D	No	S	Chronic
Altokhis et al, 2022 (43)	University of Nottingham (UK)	SC	August 2008 to July 2013	CS	MRI	SWI	7 T	3D	No	NA	Acute and chronic
Barletta et al, 2023 (45)	Massachusetts General Hospital (USA)	SC	NA	CS	PET	NA	NA	NA	NA	NA	Chronic
Barquero et al, 2020 (40)	Ecole Polytechnique Fédérale de Lausanne (Switzerland)	MC	December 2017 to September 2019	CS	MRI	T2*w	3 T	3D	No	NA	Acute and chronic
Blindenbacher et al, 2020 (39)	University of Basel (Switzerland)	MC	NA	CS and L	MRI	SWI	3 T	3D	No	NA	Acute and chronic separately
Cagol et al, 2024 (16)	University of Basel (Switzerland)	MC	January 2012 to March 2022	CS	MRI	T2*w	3 T	3D	No	NA	Chronic
Calvi et al, 2023 (46)	University College London (UK)	MC	NA	CS	MRI	SWI	3 T	2D	No	NA	Acute and chronic
Chawla et al, 2016 (47)	New York University (USA)	MC	NA	CS	MRI	QSM	7 T	2D	No	S	Acute and chronic
Clark et al, 2023 (29)	University of Pennsylvania (USA)	SC	NA	CS and L	MRI	T2*w	7 T	3D	No	S	Acute and/or acute and chronic separately
Clarke et al, 2024 (37)	Vanderbilt University Medical Center (USA)	SC	September 2020 to February 2022	CS	MRI	SWI	7 T	2D	Yes	NA	Chronic
Coffman et al, 2022 (48)	Wayne State University (USA)	SC	NA	CS and L	MRI	Other	3 T	2D	No	NA	Acute and chronic
Comabella et al, 2022 (49)	Universitat Autònoma de Barcelona (Spain)	SC	NA	CS	MRI	SWI	3 T	2D	No	S	Chronic
Dal Bianco et al, 2021 (11)	Medical University of Vienna (Austria)	SC	2010 to 2018	CS and L	MRI	SWI	7 T	2D	No	S	Chronic
Eisele et al, 2019 (42)	University of Heidelberg (Germany)	SC	NA	CS	MRI	SWI	3 T	2D	No	NA	Chronic
Elliott et al, 2023 (50)	NeuroRx Research (Canada)	MC	NA	CS	MRI	SWI	3 T	3D	No	NA	Chronic
Guo et al, 2021 (14)	Sun Yat-sen University (China)	SC	NA	CS	MRI	QSM	3 T	2D	No	WB	Acute and chronic
Haacke et al, 2009 (51)	Wayne State University (USA)	SC	NA	CS	MRI	SWI	1.5 T, 3 T, 4 T	2D, other	No	Slab of 64 sections	Acute and chronic
Hagemeier et al, 2012 (52)	University at Buffalo (USA)	SC	NA	CS	MRI	SWI	3 T	Other	No	Slab of 64 sections	Acute and chronic
Hammond et al, 2008 (53)	University of California San Francisco (USA)	SC	NA	CS	MRI	T2*w	7 T	2D	No	NA	Acute and chronic
Hemond et al, 2022 (44)	University of Massachusetts (USA)	SC	NA	CS	MRI	SWI	3 T	2D	No	NA	Chronic

(Table 1 continues)

Table 1 *(continued)*: Study Characteristics

Study and Year	Institution	SC or MC	Enrollment Dates	Study Design	Method	MRI Sequence	Field Strength	Resolution	PRL Definition with NAIMS	Brain Compartment	Lesion Stage Considered
Hu et al, 2022 (54)	Chongqing Medical University (China)	SC	January 2019 to April 2021	CS	MRI	QSM	3 T	2D	No	S	Chronic
Huang et al, 2022 (55)	Weill Cornell Medicine (USA)	SC	October 24, 2013, to April 19, 2015	CS	MRI	T2*w, QSM	3 T	2D	No	WB	Chronic
Jang et al, 2020 (31)	The Catholic University of Korea (Korea)	SC	January 2015 to December 2018	CS and L	MRI	QSM	3 T	NA	No	WB	Acute and chronic
Kaunzner et al, 2019 (56)	Weill Cornell Medicine (USA)	SC	NA	CS	MRI	QSM	3 T	2D	No	WB	Chronic
Kilsdonk et al, 2014 (57)	VU University Medical Center (The Netherlands)	SC	NA	CS	MRI	T2*w	7 T	2D	No	S	Acute and chronic
Kim et al, 2023 (58)	Chungnam National University College of Medicine (Korea)	SC	NA	CS	MRI	SWI	3T	NA	No	S	Acute and chronic
Kollia et al, 2009 (59)	University Hospital Essen (Germany)	SC	NA	CS	MRI	T2*w	7T	2D	NA	WB	Acute and chronic
Krajnc et al, 2023 (60)	Medical University of Vienna (Austria)	SC	NA	CS	MRI	SWI	3T	2D	No	WB	Acute and chronic
Kwong et al, 2022 (61)	University of Edinburgh (UK)	MC	NA	CS	MRI	SWI	3T	3D	No	WB	Chronic
Lehto et al, 2023 (27)	Turku University Hospital (Finland)	SC	December 2017 to December 2020	CS and L	MRI, PET	QSM	3T	NA	No	NA	Chronic
Lipka et al, 2023 (28)	Medical University of Vienna (Vienna)	SC	January 2016 to December 2017	CS and L	MRI	SWI	7T	2D	No	NA	Acute and chronic and/or acute
Maggi et al, 2020 (62)	Université Catholique de Louvain (Belgium)	MC	2013 to early 2020	CS	MRI	T2*w	3 T	3D	No	S	Chronic
Maggi et al, 2021 (63)	Université Catholique de Louvain (Belgium)	MC	December 2017 to September 2019	CS	MRI	T2*w	3 T	3D	No	NA	Chronic
Maggi et al, 2023 (36)	Université Catholique de Louvain (Belgium)	MC	March 2012 to September 2022	CS and L	MRI	T2*w	3 T	3D	Yes	S	Chronic
Margoni et al, 2023 (23)	IRCCS Ospedale San Raffaele (Italy)	SC	June 2018 to October 2022	CS	MRI	SWI	3 T	2D	No	NA	Acute and chronic
Meaton et al, 2022 (7)	University of Nottingham (UK)	MC	2010 to 2016	CS	MRI	SWI	3 T	Other	No	S	Acute and chronic
Micheletti et al, 2022 (24)	Hospital de Pediatría J. P. Garrahan Buenos Aires (Argentina)	SC	January 2018 to December 2019	CS	MRI	SWI	1.5 T	Other	No	S	Acute and chronic
Naval-Baudin et al, 2023 (64)	Hospital Universitari de Bellvitge (Spain)	SC	August 1, 2019, to June 9, 2020	CS	MRI	SWI	3 T	2D	No	NA	Chronic

(Table 1 continues)

Table 1 *(continued)*: Study Characteristics

Study and Year	Institution	SC or MC	Enrollment Dates	Study Design	Method	MRI Sequence	Field Strength	Resolution	PRL Definition with NAIMS	Brain Compartment	Lesion Stage Considered
Nylund et al, 2022 (65)	Turku University Hospital (Finland)	SC	NA	CS	PET	NA	NA	NA	NA	NA	Chronic
Oh et al, 2021 (66)	University of Toronto (Canada)	SC	July 2017 to August 2018	CS	MRI	T2*w	3 T	3D	No	NA	Acute and chronic
Pinto et al, 2022 (67)	AZ Sint-Jan Hospital Brugge-Oostende (Belgium)	SC	July 2020 to January 2021	CS	MRI	SWI	3 T	3D	No	WB	Acute and chronic
Rahmanzadeh et al, 2022 (68)	University of Basel (Switzerland)	MC	NA	CS	MRI	QSM	3 T	3D	No	NA	Chronic
Reeves et al, 2023 (69)	University at Buffalo (USA)	MC	NA	CS	MRI	QSM	3 T	NA	Yes	NA	Chronic
Sacco et al, 2023 (25)	University of California San Francisco (USA)	SC	2014 to 2022	CS	MRI	SWI	1.5 T/3 T	Other	No	WB	Chronic
Shi et al, 2023 (70)	Chongqing Medical University (China)	SC	April 2019 to August 2021	CS	MRI	QSM	3 T	2D	No	S	Chronic
Sinnecker et al, 2012 (71)	Charité-Universitaetsmedizin Berlin (Germany)	MC	NA	CS	MRI	T2*w	7 T	2D	No	S	Acute and chronic
Suzuki et al, 2011 (72)	Iwate Medical University (Japan)	SC	July 1, 2009, to February 28, 2010	CS	MRI	SWI	3 T	Other	No	S	Acute
Tolaymat et al, 2020 (73)	University of Maryland School of Medicine (USA)	MC	NA	CS	MRI	QSM	7 T	3D	No	NA	Acute and chronic
Tozlu et al, 2021 (74)	Weill Cornell Medicine (USA)	SC	NA	CS	MRI	QSM	3 T	2D	No	WB	Acute and chronic
Tranfa et al, 2022 (35)	University of Naples "Federico II" (Italy)	SC	October 2015 to October 2020	CS	MRI	T2*w	3 T	2D	No	WB	Acute and chronic
Treaba et al, 2021 (26)	Massachusetts General Hospital (USA)	SC	2009 to 2019	CS and L	MRI	T2*w	7 T	2D	No	S	Acute and chronic
Vanheule et al, 2024 (75)	AZ Sint-JanBrugge-Oostende (Belgium)	SC	July 2020 to March 2022	CS	MRI	SWI	3 T	3D	No	NA	Acute and chronic
Wang et al, 2023 (76)	Chongqing Medical University (China)	SC	May 2020 to June 2022	CS	MRI	QSM	3 T	2D	No	NA	Acute and chronic
Weber et al, 2022 (77)	University of Heidelberg (Germany)	SC	NA	CS	MRI	SWI	3 T	2D	No	WB	Chronic
Yao et al, 2012 (78)	National Institutes of Health (USA)	SC	January 2009 to December 2010	CS	MRI	T2*w	7 T	2D	No	NA	Chronic
Yao et al, 2018 (30)	Weill Cornell Medicine (USA)	SC	October 2011 to April 2015	CS and L	MRI	QSM	3 T	2D	No	NA	Chronic
Zhang et al, 2019 (79)	Weill Cornell Medicine (USA)	SC	2011 to 2018	CS and L	MRI	QSM	3 T	Other	No	NA	Acute and/or chronic
Zhang et al, 2022 (80)	Weill Cornell Medicine (USA)	SC	NA	CS	MRI	QSM	3 T	2D	No	NA	Acute and chronic

Note.—CS = cross-sectional, L = longitudinal, MC = multicenter, NA = not available, NAIMS = North American Imaging in Multiple Sclerosis Cooperative, PRL = paramagnetic rim lesion, QSM = quantitative susceptibility mapping, S = supratentorial, SC = single center, SWI = susceptibility-weighted imaging, T2*w = T2*-weighted, 3D = three-dimensional, 2D = two-dimensional, WB = whole brain.

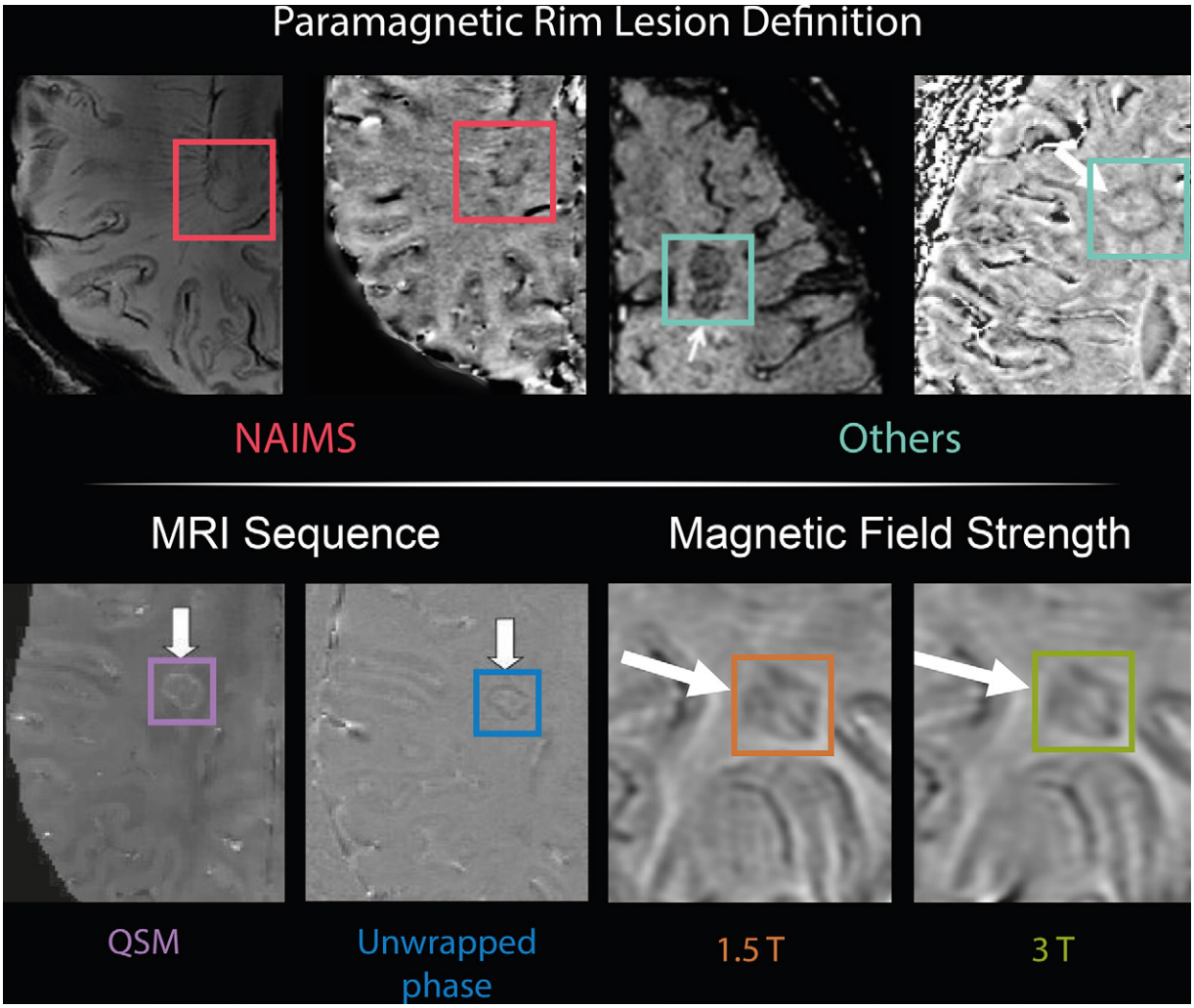

Figure 2: Methodological and technical factors affecting paramagnetic rim lesion (PRL) identification. Example MRI scans in patients with multiple sclerosis (MS) and PRLs identified using different PRL definitions, MRI sequences, and magnetic field strengths are shown. On the top row, red boxes indicate PRLs defined according to the North American Imaging in Multiple Sclerosis (NAIMS) guidelines (left: axial susceptibility-weighted image; right: axial unwrapped phase image in a 31-year-old with primary progressive MS) (22,36), whereas turquoise boxes highlight PRLs identified using criteria that do not adhere to these guidelines (left: PRL defined as "lesions with peripheral hypointense dots/rims" [42] at the axial postcontrast susceptibility weighted imaging; right: PRL defined as "hypointense rim that surrounds more than 50% of the lesion margin and visible on at least three slices" [43] at the axial susceptibility-weighted imaging–filtered phase) (42,43). On the bottom row, purple and blue boxes highlight the same PRL identified on axial quantitative susceptibility mapping (QSM) and unwrapped phase images, respectively (16). Orange and green boxes indicate the same PRL identified in a 28-year-old woman with MS using axial susceptibility-weighted imaging at 1.5 T and 3 T magnetic field strength, respectively (44). Images were adapted, under a CC BY license, from references 16, 36, 37, and 42–44.

Three studies enrolling pediatric-onset MS were identified. Their results were not included in the final analysis and are reported descriptively. The sample size of MRI studies with a cross-sectional component included in the analysis ranged from 11 to 445. Most studies analyzed both patients with relapsing-remitting MS and those with progressive MS. The proportion of female participants ranged from 44% to 89% (mean age per study, 30–51 years; mean disease duration, 0.2–19.8 years). The sample size of longitudinal studies included in the analysis ranged from 12 to 72 patients, with most studies including both patients with relapsing-remitting MS and those with progressive MS. The proportion of female participants in longitudinal studies ranged from 51% to 79% (mean age, 34.0–46.1 years; mean disease duration, 1.5–10.8 years). See Table 2 for details on patient characteristics.

Quality Assessment

In almost all studies, the sample was adequately described (98%, 57 of 58); however, the sample was representative of the target population in only about two-thirds of the studies (62%, 36 of 58), and in only a very small percentage the sample size was appropriately justified (3%, two of 58). Across studies, inclusion criteria were more frequently defined (66%, 38 of 58) compared with exclusion criteria (29%, 17 of 58). In most studies, the recruitment strategy was random (79%, 46 of 58) and the study design was retrospective (62%, 36 of 58). More than half of the studies provided a clear definition of PRLs (79%, 46 of 58), whereas there was a lack of a clear definition of PRLs in 21% of studies (12 of 58). Most studies involved more than one rater (78%, 45 of 58), but in most studies, there was no mention of the raters' level of expertise (66%, 38 of 58) or any measures of interrater and

Table 2: Participant Characteristics

Study and Year	Type of MS	No. of Patients	M:F Ratio	Mean Age (y)*	Mean Disease Duration (y)*	Therapy
Absinta et al, 2019 (9)	Mixed	92	23:69	46.6 ± 12.6	13.0 ± 10.8	NA
Altokhis et al, 2022 (43)	Mixed	91	38:53	46.1 ± 11.6	8.6 ± 8.1	NA
Barletta et al, 2023 (45)	Mixed	38	9:29	48.5 ± 9.5	14.3 ± 11.7	HET
Barquero et al, 2020 (40)	Mixed	124	47:77	45.0 ± 13.1	NA	NA
Blindenbacher et al, 2020 (39)	Mixed	66	26:40	34.0 ± 8.6	1.5 ± 1.3	None
Cagol et al, 2024 (16)	Mixed	445†	156:289	45.0 ± 11.4	11.4 ± 9.1	NA
Calvi et al, 2023 (46)	Mixed	61	19:42	35.18 ± 10.9	1.6 ± 3.6	NA
Chawla et al, 2016 (47)	Mixed	21	6:15	47.1 ± 10.3	11.5 ± 5.9	NA
Clark et al, 2023 (29)	Mixed	23	7:16	36.37 ± 10.88	9.3 ± 9.3	NA
Clarke et al, 2024 (37)	Mixed	32	18:14	37.8 ± 8.3	NA	NA
Coffman et al, 2022 (48)	R-R	43	15:28	41.0 ± 10.0	10.3 ± 8.6	NA
Comabella et al, 2022 (49)	Mixed	61	16:45	36.4 ± 9.9	0.2 ± 0.2	NA
Dal Bianco et al, 2021 (11)	Mixed	33	16:17	37.3 ± 10.6	8.6 ± 7.5	LET
Eisele et al, 2019 (42)	Mixed	294	68:226	36.0	NA	NA
Elliott et al, 2023 (50)	Mixed	41	14:27	38.2 ± 12.4	5.8 ± 6.1	NA
Guo et al, 2021 (14)	R-R	26	14:12	29.0 ± 8.0	5.7 ± 4.8	NA
Haacke et al, 2009 (51)	Mixed	27	6:21	45	NA	NA
Hagemeier et al, 2012 (52)	Mixed	135	34:101	46.7 ± 10.2	14.6 ± 9.8	NA
Hammond et al, 2008 (53)	R-R	19	6:13	42.3 ± 12.9	12.0 ± 7.6	NA
Hemond et al, 2022 (44)	Mixed	147	78:69	48.8 ± 11.7	12.8 ± 9.8	NA
Hu et al, 2022 (54)	R-R	42	8:34	31.2 ± 9.2	4.3 ± 5.2	None
Huang et al, 2022 (55)	R-R	80	24:56	41.8 ± 9.7	9.3 ± 5.5	NA
Jang et al, 2020 (31)	R-R	32	7:25	35.0 ± 10.6	2.8 ± 4.10	NA
Kaunzner et al, 2019 (56)	Mixed	30	12:18	43.8 ± 14.3	13.1 ± 11.9	HET
Kilsdonk et al, 2014 (57)	Mixed	33	13:20	44.2 ± 8.4	9.6 ± 5.9	NA
Kim et al, 2023 (58)	Mixed	30	13:17	30.9 ± 11.0	6.4 ± 6.2	NA
Kollia et al, 2009 (59)	Mixed	12	4:8	32.0	5 (1–10)‡	NA
Krajnc et al, 2023 (60)	Mixed	107	38:69	34.7 ± 10.9	6.7 ± 9.0	HET
Kwong et al, 2022 (61)	R-R	44	11:33	42.6 ± 12.8	4.9 ± 5.0	LET
Lehto et al, 2023 (27)	R-R	12	3:9	46.1 ± 6.2	10.8 ± 8.1	LET
Lipka et al, 2023 (28)	R-R	31	15:16	36.9 ± 10.3	9.1 ± 5.2	None
Maggi et al, 2020 (62)	Mixed	329	131:198	45.0	NA	NA
Maggi et al, 2021 (63)	Mixed	118	NA	NA	NA	NA
Maggi et al, 2023 (36)	Mixed	72	28:44	NA	NA	HET
Margoni et al, 2023 (23)	POMS	13	2:11	15.1 ± 3.48	1.1 ± 1.2	NA
Meaton et al, 2022 (7)	Mixed	254	85:169	NA	NA	NA
Micheletti et al, 2022 (24)	POMS	13	2:11	15.0 ± 2.5	NA	NA
Naval-Baudin et al, 2023 (64)	Mixed	20	6:14	51.2 ± 6.15	19.8 ± 6.8	NA
Nylund et al, 2022 (65)	Mixed	91	21:70	44.9 ± 9.67	11.7 ± 6.4	NA
Oh et al, 2021 (66)	RIS	27	6:21	45.0 ± 11.3	NA	NA
Pinto et al, 2022 (67)	Mixed	192	70:122	46.2	10.1	HET
Rahmanzadeh et al, 2022 (68)	Mixed	115	48:67	46.0 ± 14.0	9.2 ± 10.4	HET
Reeves et al, 2023 (69)	R-R	42	10:32	NA	NA	LET
Sacco et al, 2023 (25)	POMS	26	10:16	14.7 ± 3.13	0.1 ± 0.2	NA
Shi et al, 2023 (70)	R-R	68	12:56	29.9 ± 9.3	3.9 ± 5.1	None
Sinnecker et al, 2012 (71)	R-R	18	7:11	41.0 ± 8.0	6.6 ± 5.8	NA
Suzuki et al, 2011 (72)	R-R	11	3:8	32.0	4.6	NA
Tolaymat et al, 2020 (73)	Mixed	39	15:24	46.5 ± 11.1	12.3 ± 8.6	LET
Tozlu et al, 2021 (74)	Mixed	96	32:64	40.2 ± 10.1	6.2 ± 6.6	NA
Tranfa et al, 2022 (35)	R-R	73	8:65	38.6 ± 11.2	8.7 ± 6.3	NA
Treaba et al, 2022 (26)	Mixed	100	24:76	NA	NA	HET
Vanheule et al, 2023 (75)	Mixed	84	31:53	46.0 ± 11.78	NA	HET
Wang et al, 2023 (76)	R-R	99	18:81	33.6 ± 10.0	2.83 (6.67)§	None
Weber et al, 2022 (77)	R-R	102	26:76	NA	NA	NA

(Table 2 continues)

Table 2 (*continued*): Participant Characteristics

Study and Year	Type of MS	No. of Patients	M:F Ratio	Mean Age (y)*	Mean Disease Duration (y)*	Therapy
Yao et al, 2012 (78)	Mixed	21	11:10	46.2	NA	NA
Yao et al, 2018 (30)	Mixed	46	14:32	43.6 ± 10.7	8.7 ± 7.0	NA
Zhang et al, 2019 (79)	R-R	19	4:15	36.3 ± 6.4	4.8 ± 3.2	NA
Zhang et al, 2022 (80)	Mixed	172	48:124	42.8 ± 10.3	10.7 ± 7.4	NA

Note.—A population is defined "mixed" when it includes more than one phenotype. Therapy classification was achieved considering the treatments ongoing in more than 50% of each population. HET = moderate-high efficacy (alemtuzumab, cladribine, fingolimod, natalizumab, ocrelizumab, ofatumumab, ozanimod, ponesimod, rituximab, and siponimod), LET = low-moderate efficacy (dimethyl fumarate, glatiramer acetate, interferon β-1a, interferon β-1b, pegylated interferon β-1a, teriflunomide), MS = multiple sclerosis, NA = not available, POMS = pediatric-onset MS, R-R = relapsing-remitting, RIS = radiologically isolated syndrome.

* Data are means ± SDs. For studies that reported medians and IQRs, means and SDs were estimated.

† The sample size reported refers to the enrolled population, for which demographic data are available. PRL analysis was then conducted for 443 patients, as indicated in Figure 4.

‡ Data are medians with the range in parentheses.

§ Data are medians with IQR in parentheses.

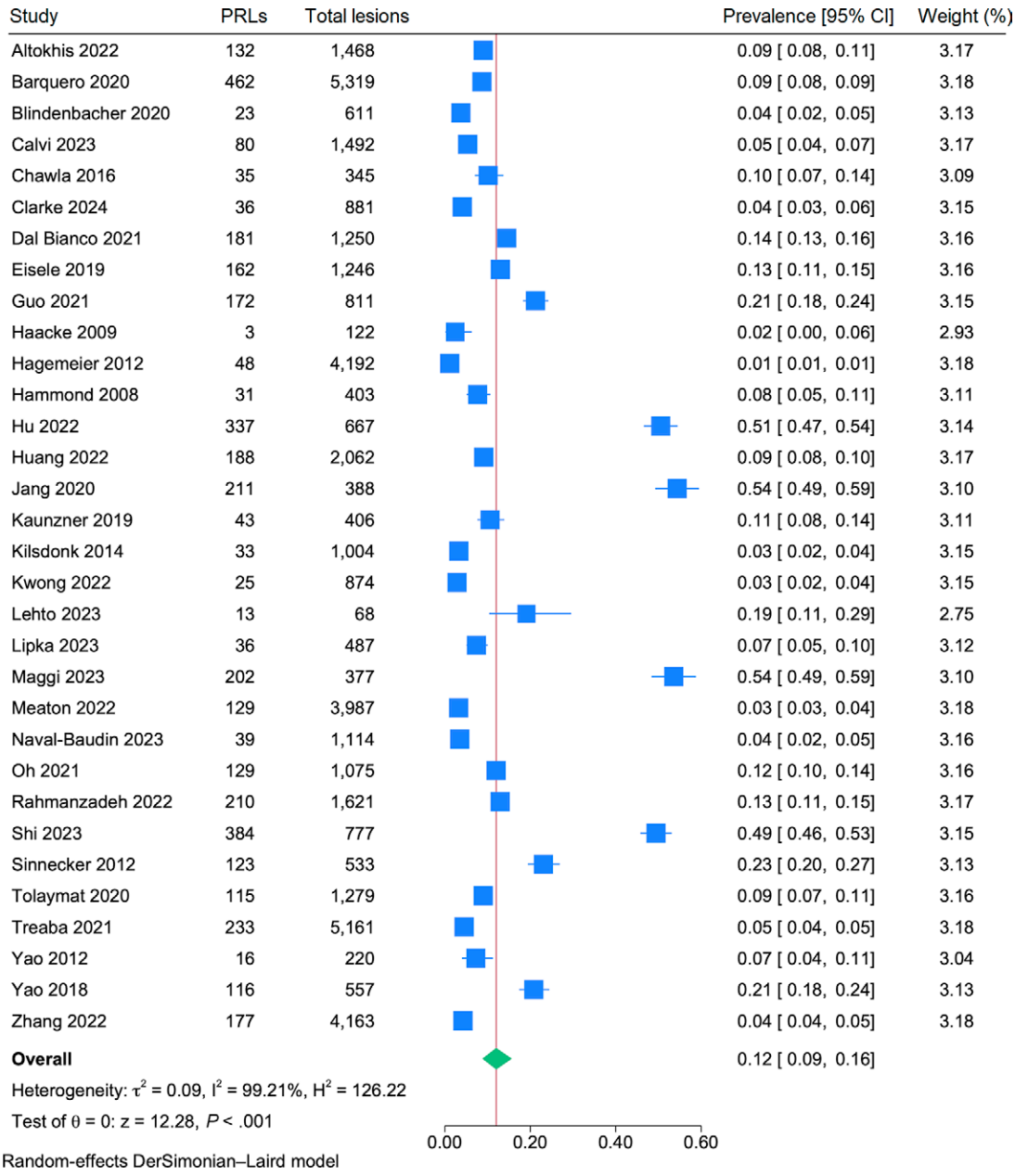

Figure 3: Forest plot of paramagnetic rim lesion (PRL) prevalence across 32 studies. Pooled prevalence was 0.12. The area of each blue square is proportional to the study's weight in the pooled analysis, based on variance and sample size. Horizontal lines represent 95% CI values of the point estimates. The green diamond represents the pooled estimate (size of the diamond = 95% CI). The vertical line represents the overall point estimate determined with the random effects model. Heterogeneity was assessed using the Cochran Q test and the I^2 statistic.

intrarater reliability (78%, 45 of 58) (see Appendix S1 for details). Statistical analyses were generally appropriately described (67%, 39 of 58). Heterogeneity assessed using the I^2 statistic was generally high. For PRL lesion- and patient-level prevalence, I^2 was 99.2% and 88.8%, respectively. Similarly, I^2 was 99.2% for PRL prevalence across studies using different PRL definitions, field strengths, MRI sequences, and resolutions. I^2 was 99.1% and 87.6% for lesion- and patient-level prevalence, respectively, among studies including different clinical phenotypes.

Prevalence Rates of PRLs

The number of PRLs was reported in 32 of the 58 studies (2185 patients). Overall, the lesion-level pooled prevalence of PRLs was 0.12 (95% CI: 0.09, 0.16) and the I^2 value was 99.2% (Fig 3). The number of patients with at least one PRL was reported in 37 of the 58 studies (3180 patients), with a pooled prevalence of 0.52 (95% CI: 0.47, 0.58) and an I^2 value of 88.8% (Fig 4).

Three studies (141 patients) reported the number of PRLs using PET, with a lesion-level pooled prevalence of 0.17 (95% CI: 0.13, 0.21) and a heterogeneity of 87.4%. Two studies (103

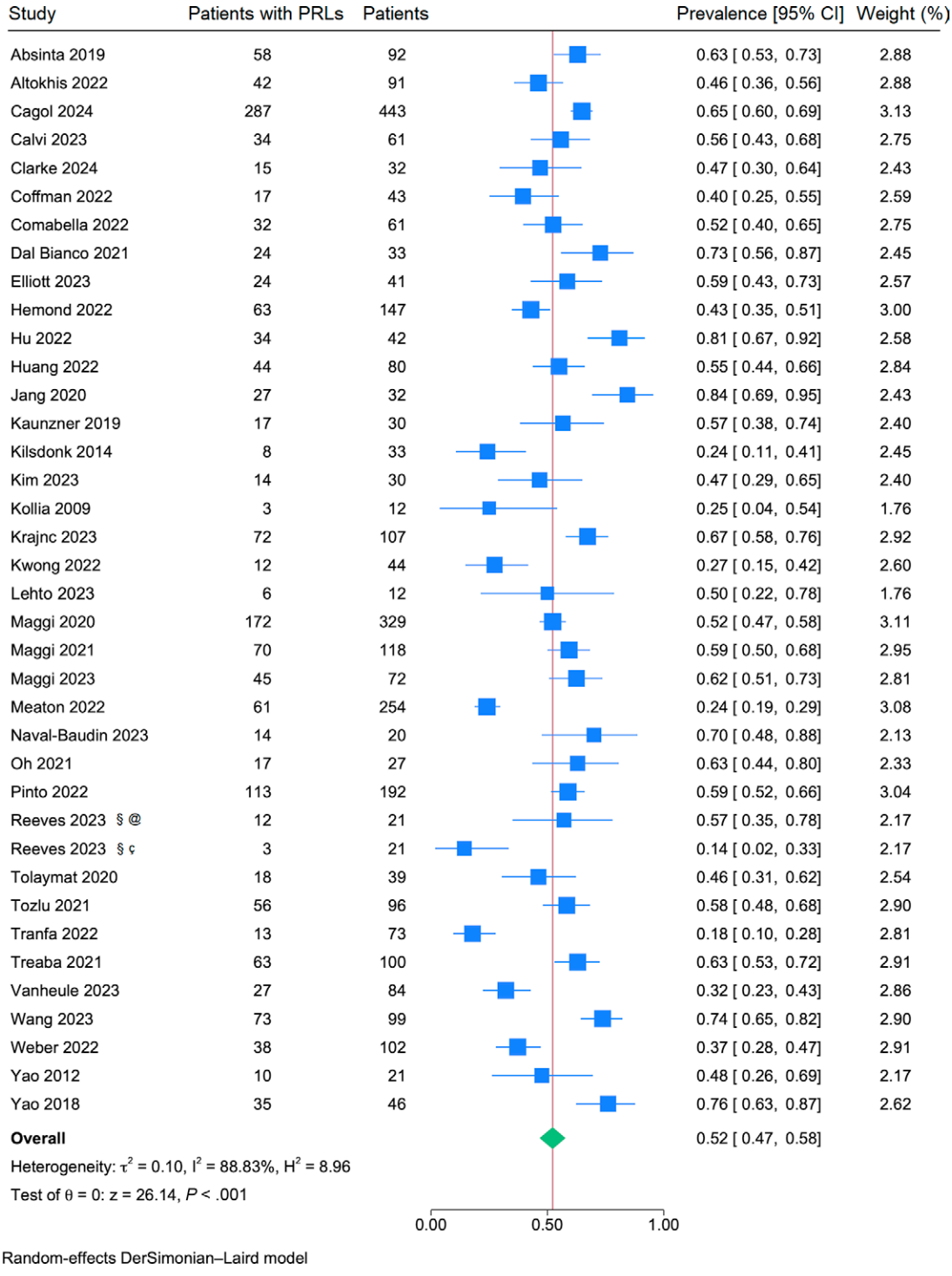

Figure 4: Forest plot shows the prevalence of patients with at least one paramagnetic rim lesion (PRL) across 37 studies. Pooled prevalence was 0.52. The area of each blue square is proportional to the study's weight in the pooled analysis, based on variance and sample size. Horizontal lines represent 95% CI values of the point estimates. The green diamond represents the pooled estimate (size of the diamond = 95% CI). The vertical line represents the overall point estimate determined by the random effects model. Heterogeneity was assessed using the Cochran Q test and the I^2 statistic. § = same study, @ = patients with relapsing-remitting multiple sclerosis with at least one relapse, ç = stable patients with relapsing-remitting MS.

Table 3: Topography of PRLs

Study and Year	PV	Deep WM	JC	Deep GM	IC	MIX	CL	WML	ST	IT	FL	PL	TL	OL	CBL
Dal Bianco et al, 2021 (11)	43/181 (23.8)	136/181 (75.1)	2/181 (1.1)	NA	NA	NA	NA	NA	NA	NA	NA	NA	NA	NA	NA
Guo et al, 2021 (14)	63/172 (36.6)	42/172 (24.4)	64/172 (37.2)	NA	NA	NA	NA	NA	NA	3/172 (1.7)	NA	NA	NA	NA	NA
Jang et al, 2020 (31)	NA	NA	NA	NA	NA	NA	NA	NA	211/211 (100.0)	0/211 (0.0)	NA	NA	NA	NA	NA
Kaunzner et al*, 2019 (56)	NA	NA	NA	NA	NA	NA	NA	NA	NA	NA	(28)	(23)	(32)	(14)	(3)
Kilsdonk et al, 2014 (57)	6/33 (18.2)	3/33 (9.1)	11/33 (33.3)	NA	1/33 (3.0)	12/33 (36.4)	NA	NA	NA	NA	NA	NA	NA	NA	NA
Kwong et al, 2022 (61)	NA	NA	NA	NA	NA	NA	NA	NA	24/25 (96.0)	1/25 (4.0)	NA	NA	NA	NA	NA
Meaton et al†, 2022 (7)	NA	61/72 (84.7)	NA	NA	NA	NA	NA	NA	NA	NA	NA	NA	NA	NA	NA
Micheletti et al, 2022 (24)	12/45 (26.7)	22/45 (48.9)	11/45 (24.4)	NA	NA	NA	NA	NA	NA	NA	NA	NA	NA	NA	NA
Pinto et al, 2022 (67)	369/543 (68.0)	157/543 (28.9)	9/543 (1.7)	4/543 (0.7)	NA	NA	NA	NA	539/543 (99.3)	4/543 (0.7)	NA	NA	NA	NA	NA
Sacco et al, 2023 (25)	24/55 (43.6)	7/55 (12.7)	22/55 (40.0)	NA	NA	NA	NA	NA	53/55 (96.4)	2/55 (3.6)	NA	NA	NA	NA	NA
Treaba et al, 2021 (26)	NA	NA	NA	NA	NA	NA	14/247 (5.7)	233/247 (94.3)	NA	NA	NA	NA	NA	NA	NA
Weber et al, 2022 (77)	20/52 (38.5)	29/52 (55.8)	3/52 (5.8)	NA	NA	NA	NA	NA	NA	NA	NA	NA	NA	NA	NA

Note.—Data are numbers of PRLs in each compartment/total number of PRLs with percentages in parentheses. CBL = cerebellum, CL = cortical lesion, FL = frontal lobe, GM = gray matter, IC = intracortical, IT = infratentorial, JC = juxtacortical, MIX = mixed gray matter/white matter, NA = not applicable, OL = occipital lobe, PL = parietal lobe, PRL = paramagnetic rim lesion, PV = periventricular, ST = supratentorial, TL = temporal lobe, WM = white matter, WML = WM lesion.

* Raw numbers for lesion topography were not specified.

† Additional locations of PRLs were not reported.

patients) reported the number of patients with at least one PRL detected with PET, with a pooled prevalence of 0.59 (95% CI: 0.33, 0.84) and an I^2 value of 69.4%.

The pooled prevalence of acute lesions, determined from four studies reporting cross-sectional data (119 patients), was 0.38 (95% CI: 0.26, 0.51) with an I^2 value of 68.0%.

The three pediatric-onset MS studies (52 patients) reported PRL prevalence of 0.03 (23) or 0.71 (24), and the prevalence of patients with at least one PRL was 0.69 (25), 0.77 (23), and 0.92 (24).

Incidence Rates and Evolution over Time of PRLs

Two longitudinal studies (112 patients) reported no new PRLs over a mean follow-up ranging from 1.0 to 1.4 years (26,27).

Three studies (100 patients) reported data related to new PRL incidence at the lesion level (28–30). The pooled incidence of new PRLs during a mean follow-up of 1.5 years was 0.23 (95% CI: 0, 0.75). Only two studies (65 patients) reported data related to PRL incidence at the patient level (11,31). The pooled incidence of patients with new PRLs during a mean follow-up of 4.7 years was 0.11 (95% CI: 0, 0.47). Data regarding evolution over time of PRLs are provided in Appendix S1.

PRL Topography

Twelve studies provided information on PRL topography (885 patients). The proportion of PRLs ranged from 0.18 to 0.68 in the periventricular white matter, 0.09 to 0.85 in the deep white matter, and 0.01 to 0.40 in the juxtacortical white matter. See Table 3 for details.

Impact of Methodological Factors on PRL Lesion-level Prevalence

Subgroup analysis revealed no difference in PRL lesion-level prevalence based on adherence to the NAIMS recommendations

(32 studies, 2185 patients; P = .66) (Fig 5A) or according to brain compartment (16 studies, 1015 patients; P = .34) (Fig S1), whereas differences emerged across field strength (32 studies, 2185 patients), MRI sequences (32 studies, 2185 patients), and resolution (30 studies, 2141 patients) (P < .001 for all) (Figs 5B, 6). Post hoc analyses showed comparable pooled prevalence of PRLs between quantitative susceptibility maps and T2*-weighted imaging (P = .51), and between susceptibility-weighted imaging and T2*-weighted imaging (P = .12), with quantitative susceptibility mapping outperforming susceptibility-weighted imaging (P < .001). Three-dimensional and two-dimensional resolutions showed no evidence of a difference in PRL prevalence (P > .99) but showed higher prevalence than other resolutions (P < .001 for both). Last, 3-T and 7-T field strengths outperformed 4-T field strengths (P < .001 for both), and showed comparable performance (P = .12).

Impact of Clinical Factors on PRL Prevalence

Subgroup analysis showed no evidence of a difference in lesion-level (16 studies, 756 patients) or patient-level (21 studies, 1242 patients) PRL prevalence according to MS phenotypes (P = .22 and P = .29, respectively) (Fig 7).

Additionally, at meta-regression analysis, no association between the pooled prevalence of patients with PRLs and mean age (31 studies, 2492 patients, coefficient = −0.014; standard error = 0.010; P = .29) or disease duration (25 studies, 1987 patients, coefficient = −0.006; standard error = 0.018; P = .72) was found.

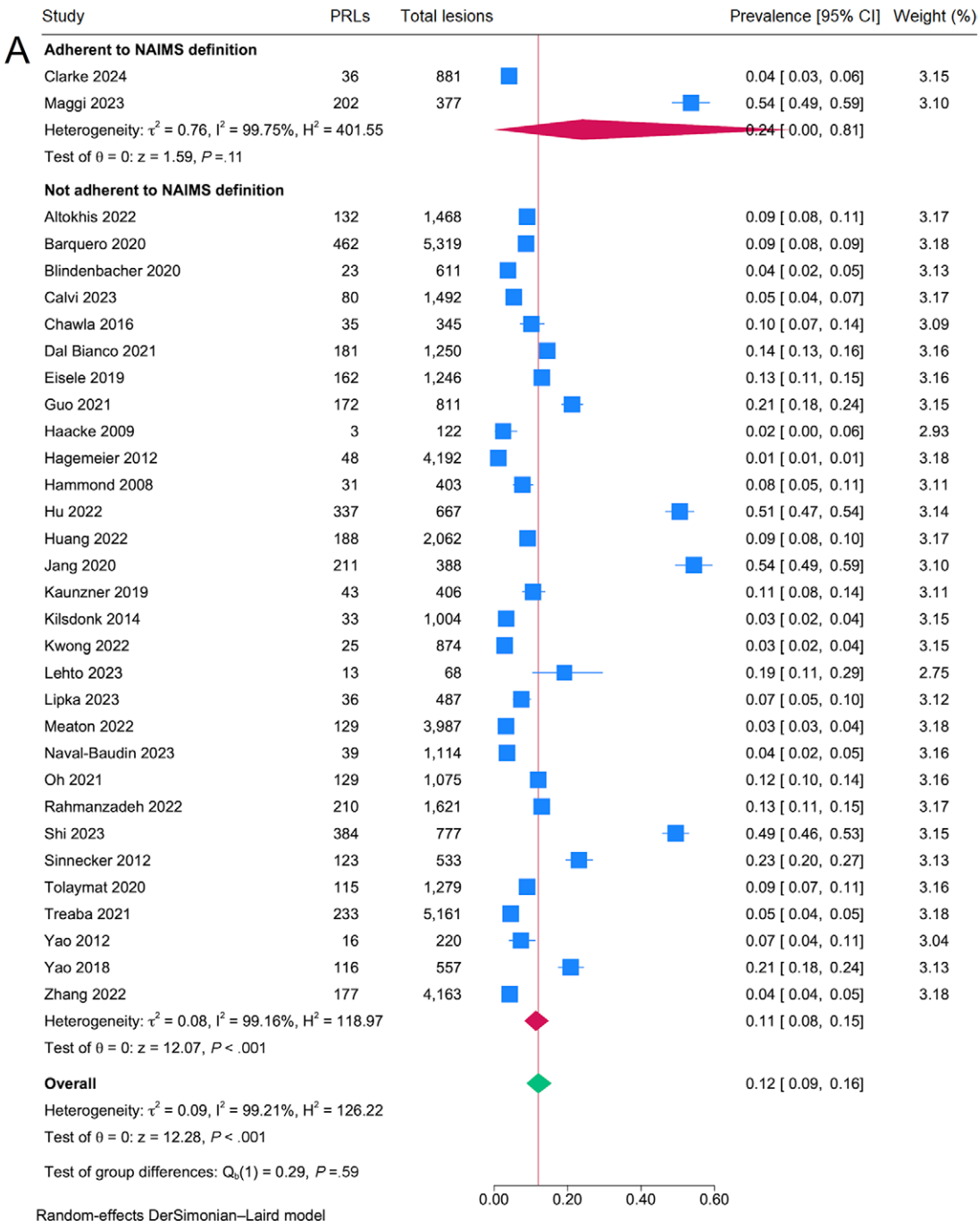

Figure 5: **(A)** Forest plot of paramagnetic rim lesion (PRL) prevalence according to different PRL definitions across 32 studies. Pooled prevalence was 0.12, with no significant differences among studies according to PRL definition (P = .66). The area of each blue square is proportional to the study's weight in the pooled analysis, based on variance and sample size. Horizontal lines represent 95% CI values of the point estimates. The red diamond represents the pooled estimate within the subgroups (size of the diamond = 95% CI). The green diamond represents the overall pooled estimate (size of the diamond = 95% CI). The vertical line represents the overall point estimate determined by the random effects model. Heterogeneity was assessed using the Cochran Q test and the I^2 statistic *(Fig 5 continues).*

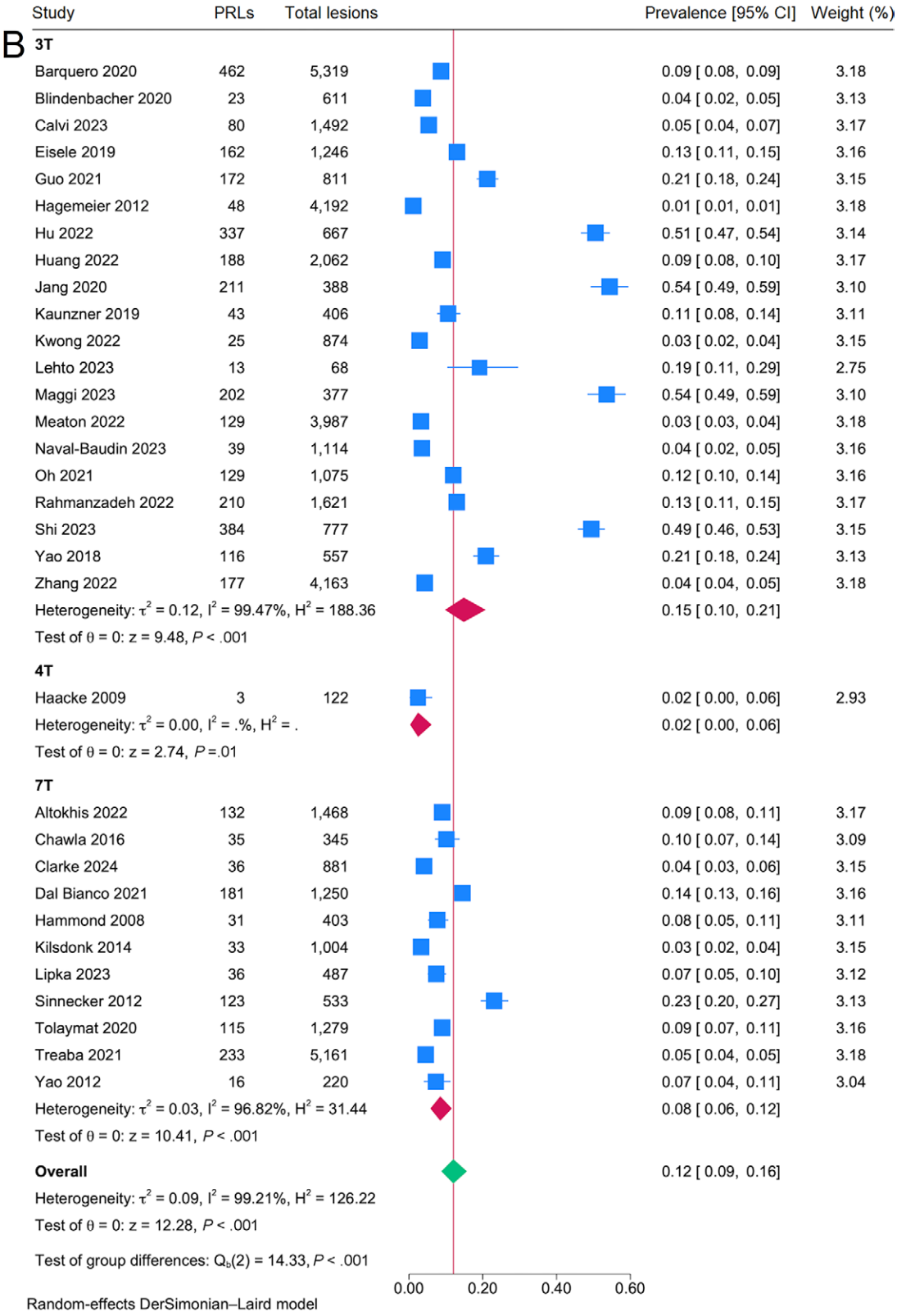

Figure 5 *(continued)*: (B) Forest plot of PRL prevalence according to different field strength across 32 studies. Pooled prevalence was 0.12, with significant differences among studies according to field strength ($P < .001$). Horizontal lines represent 95% CI values of the point estimates. The red diamond represents the pooled estimate within the subgroups (size of the diamond = 95% CI). The green diamond represents the overall pooled estimate (size of the diamond = 95% CI). The vertical line represents the overall point estimate determined by the random effects model. Heterogeneity was assessed using the Cochran Q test and the I^2 statistic. NAIMS = North American Imaging in Multiple Sclerosis.

Subgroup analysis revealed differences in lesion-level PRL prevalence between acute and chronic lesions (18 studies, 1028 patients; $P < .001$) (Fig S2).

Discussion

This systematic review and meta-analysis aimed to investigate the prevalence, incidence, and evolution of paramagnetic rim lesions (PRLs) in patients with multiple sclerosis (MS), with consideration of the impact of technical, methodological, and clinical factors on PRL detection. We included 58 studies and analyzed data from 4532 patients. The overall pooled prevalence of PRLs at the lesion level was 0.12 (95% CI: 0.09, 0.16; $P < .001$), whereas the prevalence of patients with at least one PRL was 0.52 (95% CI: 0.47, 0.58; $P < .001$). Significant differences

in lesion-level prevalence were observed across field strengths, MRI sequences, and resolutions ($P < .001$ for all), but not based on MS phenotype ($P = .22$) or adherence to North American Imaging in Multiple Sclerosis criteria ($P = .66$). The incidence of new PRLs over time was relatively low (0.23 at the lesion level and 0.11 at the patient level), reinforcing their nature as markers of chronic inflammation.

Our work highlights several critical points. First, the data on patient-level prevalence of PRLs underline how this biomarker, although specific, is not necessarily identifiable in all patients with MS, supporting the need to strive for classifications based on patients' specific pathologic features, as disease drivers may vary across individuals and over time (32–34). On the other hand, the considerable heterogeneity identified (88.8% for

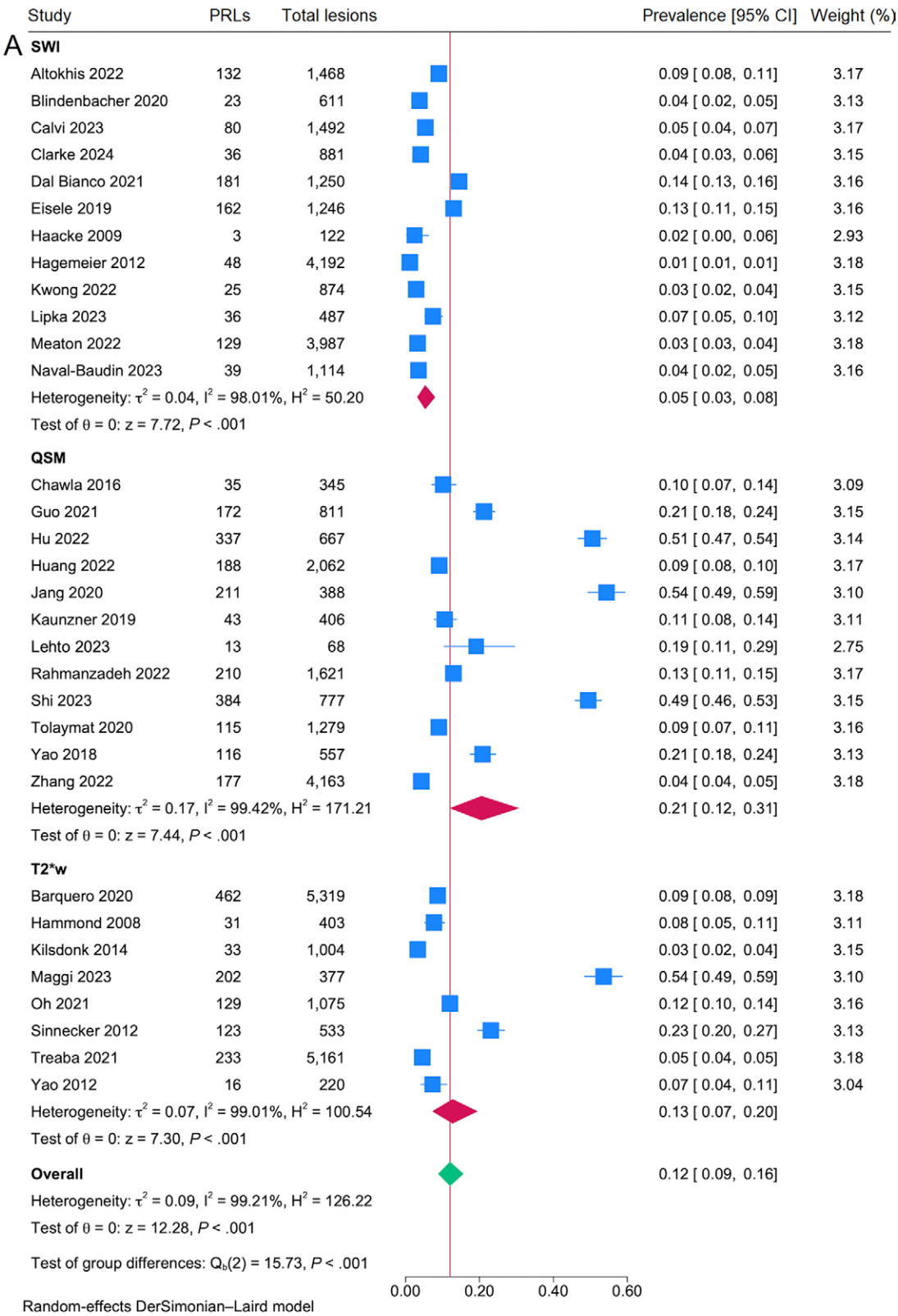

Figure 6: **(A)** Forest plot of paramagnetic rim lesion (PRL) prevalence according to the different MRI sequences across 32 studies. Pooled prevalence was 0.12, with significant differences among studies according to MRI sequence ($P < .001$). The area of each blue square is proportional to the study's weight in the pooled analysis, based on variance and sample size. Horizontal lines represent 95% CI values of the point estimates. The red diamond represents the pooled estimate within the subgroups (size of the diamond = 95% CI). The green diamond represents the overall pooled estimate (size of the diamond = 95% CI). The vertical line represents the overall point estimate determined by the random effects model. Heterogeneity was assessed using the Cochran Q test and the I^2 statistic *(Fig 6 continues).*

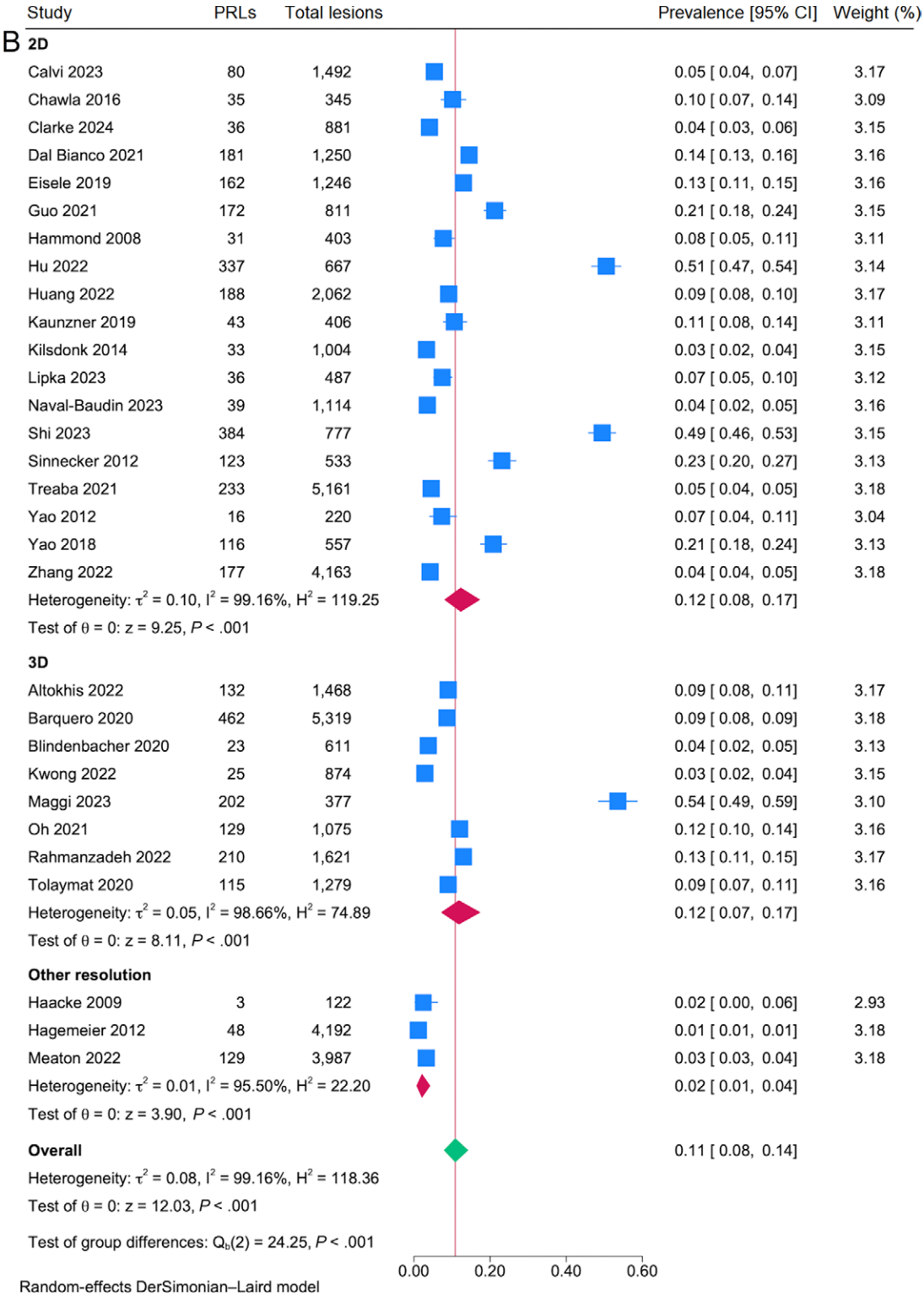

Figure 6 (*continued*): (B) Forest plot of PRL prevalence according to resolution across 30 studies. Pooled prevalence was 0.11, with significant differences among studies according to resolution ($P < .001$). The red diamond represents the pooled estimate within the subgroups (size of the diamond = 95% CI). Horizontal lines represent 95% CI values of the point estimates. The green diamond represents the overall pooled estimate (size of the diamond = 95% CI). The vertical line represents the overall point estimate determined by the random effects model. Heterogeneity was assessed using the Cochran Q test and the I^2 statistic. QSM = quantitative susceptibility mapping, SWI = susceptibility weighted imaging, 3D = three-dimensional, 2D = two-dimensional.

patient-level prevalence and 99.2% for lesion-level prevalence) points to the variability in detection methods and study designs in the field. The overall lesion-level prevalence of PRLs was affected by sequence type and field strength, further supporting this. Among MRI sequences, quantitative susceptibility mapping was associated with the highest pooled prevalence. This finding, combined with recent postmortem evidence demonstrating its high sensitivity and specificity (20) and its ability to provide quantitative measures through dipole field deconvolution, supports its preferential use over other sequences (35). Although magnetic field strength seemed to affect PRL prevalence counterintuitively, 4-T data were underrepresented, and the lack of difference between 3-T and 7-T imaging might have been driven by MRI sequence differences. Indeed, studies using 3 T more often employed quantitative susceptibility mapping than those using 7 T (10 of 20 [50%] vs two of 11 [18%]). The

high heterogeneity observed when comparing subgroups based on field strength, sequence type, and resolution might be due to inconsistencies in patients' sampling and detection strategies as well as the definition of PRLs adopted by each study. Indeed, only two of the three studies following the NAIMS guidelines assessed the prevalence of PRLs at lesion level, reporting discordant data (36,37), whereas the remaining studies adopted variable definitions or did not provide any. Inconsistencies in patients' sampling and detection strategies might also contribute to heterogeneity. In only 62% of the studies were the samples representative of the target population, and even if most of the studies (78%) included multiple raters, only a minority (22%) used measures of rater concordance.

Interestingly, acute lesions exhibited greater prevalence of paramagnetic rims compared with chronic lesions. This is in line with the biologic substrate of PRLs, which reflect inflammatory edge expansion in destructive acute lesions (38), and sustained, smoldering inflammation in chronic ones (35). When exploring clinical factors potentially affecting PRL prevalence, we found, in line with previous evidence, no impact of age and disease duration (18). Also, we did not observe any difference in lesion-level and patient-level prevalence of PRLs among radiologically

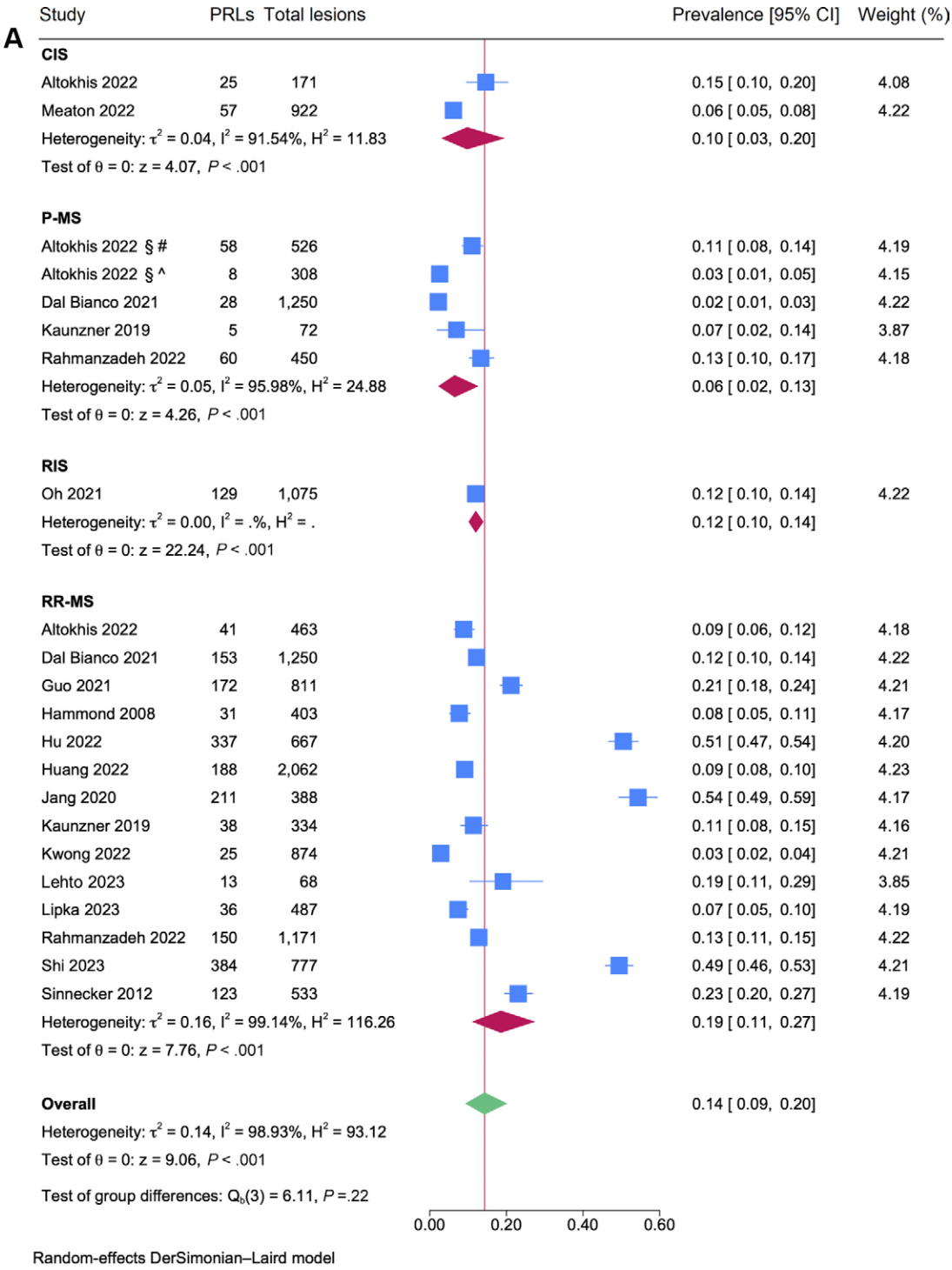

Figure 7: **(A)** Forest plot of paramagnetic rim lesion (PRL) prevalence according to different clinical phenotypes across 16 studies. Pooled prevalence was 0.14, with no significant differences among studies according to clinical phenotype (P = .22). The area of each blue square is proportional to the studies' weight in the pooled analysis, based on variance and sample size. Horizontal lines represent 95% CI values of the point estimates. The red diamond represents the pooled estimate within the subgroups (size of the diamond = 95% CI). The green diamond represents the overall pooled estimate (size of the diamond = 95% CI). The vertical line represents the overall point estimate determined by the random effects model. Heterogeneity was assessed using the Cochran Q test and the I^2 statistic *(Fig 7 continues).*

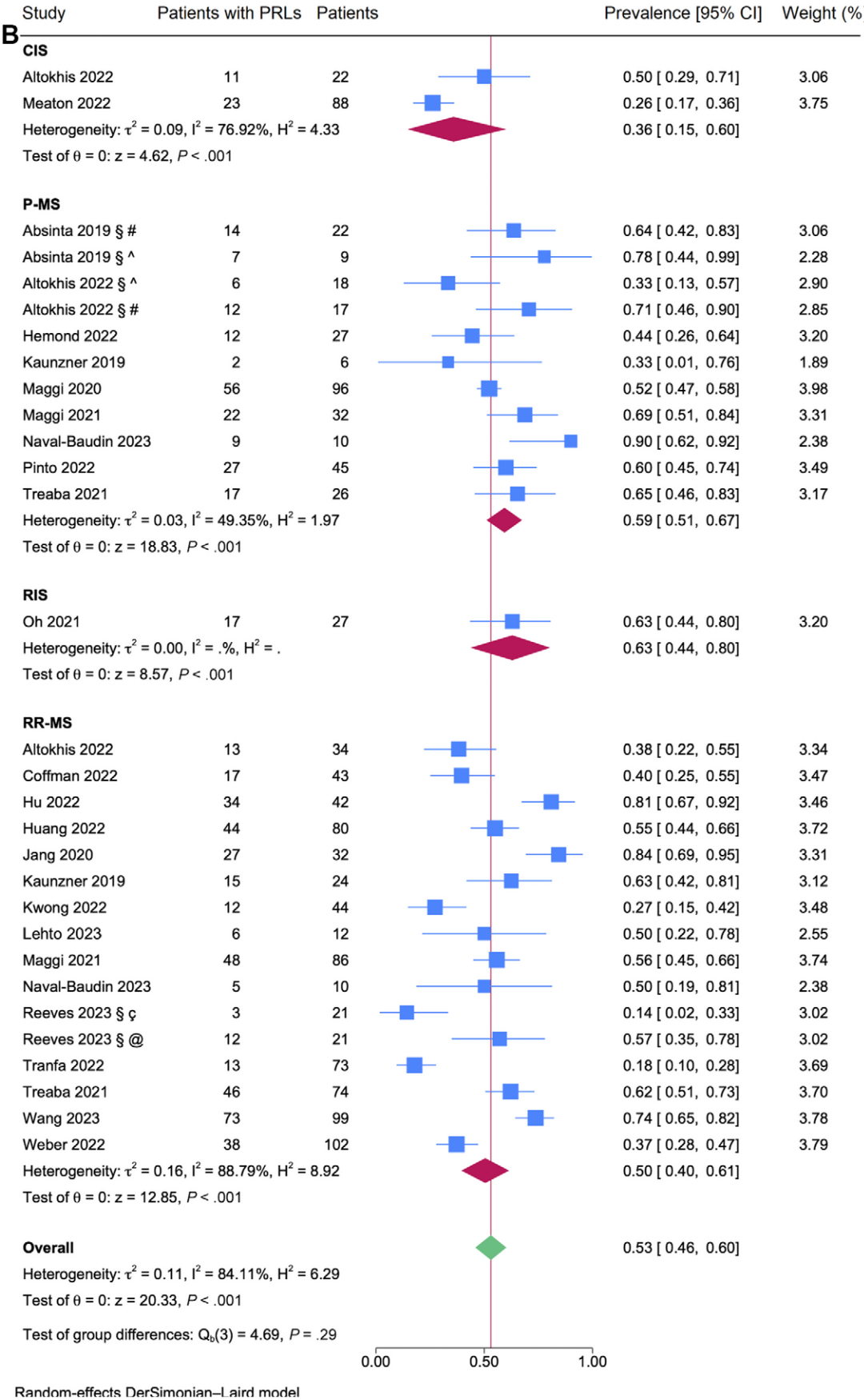

Figure 7 (*continued*): (B) Forest plot shows the prevalence of patients with at least one PRL according to different clinical phenotypes across 21 studies. Pooled prevalence was 0.53, with no significant differences among studies according to clinical phenotype (P = .29). The red diamond represents the pooled estimate within the subgroups (size of the diamond = 95% CI). Horizontal lines represent 95% CI values of the point estimates. The green diamond represents the overall pooled estimate (size of the diamond = 95% CI). The vertical line represents the overall point estimate determined by the random effects model. Heterogeneity was assessed using the Cochran Q test and the I^2 statistic. CIS = clinically isolated syndrome, MS = multiple sclerosis, P-MS = progressive MS, RIS = radiologically isolated syndrome. § = same study, # = secondary progressive, ^ = primary progressive, ç = stable patients with relapsing-remitting MS (RR-MS), @ = patients with relapsing-remitting MS with at least one relapse.

isolated syndrome, clinically isolated syndrome, and relapsing and progressive patients, suggesting that, given current methodological limitations, PRLs may not be useful for clinical phenotyping. Notably, subgroups of studies selectively including one phenotype showed significant differences and high heterogeneity concerning other parameters (ie, field strength, sequence type, resolution). Longitudinal studies reporting PRL incidence revealed that the formation of new PRLs is relatively uncommon. Although only rarely did PRLs simultaneously enhance with gadolinium-based contrast agents (39), they usually developed from lesions enhanced with gadolinium-based contrast agent administration over variable follow-up periods (8,38). PRLs demonstrated persistence over several years, with the iron rim slowly fading and with little evidence of complete resolution, further supporting their chronic and stable nature (8,11,39). Given the wide variability in the rate of PRL formation and persistence, individual factors, such as repair capabilities and ongoing treatments, likely affect PRL evolution.

Some limitations must be considered. First, data on PRL topography and evolution are sparse. Future studies are needed to elucidate the dynamics of PRL formation. Because of the limited availability of information regarding disease-modifying therapies, their potential effect could not be analyzed. Next, we acknowledge that the high methodological variability across studies certainly impacted the reliability of the pooled estimates. Very few studies adhered to the NAIMS guidelines for PRL definition and assessment, largely because these criteria were proposed only recently. Additionally, inconsistencies in imaging protocols and study populations contributed substantially to the heterogeneity of the pooled data. A promising avenue to address this issue is the integration of machine learning and deep learning, which have demonstrated excellent performance in PRL detection (40,41).

In conclusion, although paramagnetic rim lesions (PRLs) were prevalent in approximately half of patients with multiple sclerosis (MS) undergoing imaging, the incidence of new PRLs was relatively low and PRL prevalence was heterogeneous across studies. We hope the provided evidence may serve as a catalyst to overcome heterogeneity in PRL assessment in both future research and clinical settings by adopting standardized evaluation methods, in line with the recent effort of the North American Imaging in Multiple Sclerosis Cooperative (22), so that PRL assessment can be used reliably in patient management. Consistent and standardized PRL acquisition and detection protocols would enable more reliable and replicable evaluations of their prevalence and incidence. This would help clarify PRL sensitivity to disease severity and prognostic value, and their potential role in distinguishing biologically relevant MS phenotypes, as well as facilitating patient stratification for individual treatments.

Deputy Editor: Sven Haller
Scientific Editor: Kate Vilas

Author affiliations:

[1] Department of Advanced Biomedical Sciences, University of Naples Federico II, Via Pansini 5, 80131 Naples, Italy

[2] Department of Radiology and Nuclear Medicine, Amsterdam UMC, Vrije Universiteit, Amsterdam, the Netherlands

[3] Department of Neurosciences and Reproductive and Odontostomatological Sciences, University of Naples Federico II, Naples, Italy

[4] Department of Molecular Medicine and Medical Biotechnology, University of Naples Federico II, Naples, Italy

[5] Multiple Sclerosis Unit, Policlinico Federico II University Hospital, Naples, Italy

[6] Department of Anatomy and Neurosciences, MS Center Amsterdam, Amsterdam Neuroscience, Amsterdam UMC, Vrije Universiteit, Amsterdam, the Netherlands

[7] Queen Square Multiple Sclerosis Centre, Department of Neuroinflammation, UCL Queen Square Institute of Neurology, University College London, London, United Kingdom

[8] Department of Human Neurosciences, Sapienza University of Rome, Rome, Italy

Received December 6, 2024; revision requested January 10, 2025; final revision received July 9; accepted July 30.

Address correspondence to: S. Cocozza (email: sirio.cocozza@unina.it).

Funding: Authors declared no funding for this work.

Acknowledgment: The authors would like to thank Luca Prosperini, MD, PhD, for his contribution to the statistical analysis.

Author contributions: Guarantors of integrity of entire study, **M. Tranfa, M.P.**; study concepts/study design or data acquisition or data analysis/interpretation, all authors; manuscript drafting or manuscript revision for important intellectual content, all authors; approval of final version of submitted manuscript, all authors; agrees to ensure any questions related to the work are appropriately resolved, all authors; literature research, **M. Tranfa, G.C., A. Cuocolo, M.M., A.S., M. Tarantino, G.P., S. Cocozza, M.P.**; clinical studies, **R.L., M. Tarantino**; experimental studies, **S. Capasso, M. Tarantino, F.T.**; statistical analysis, **M. Tranfa, V.C., R.G., A. Cuocolo, M. Tarantino, G.P.**; and manuscript editing, **M. Tranfa, V.C., R.G., A. Carotenuto, A. Cuocolo, M.M., A.S., M. Tarantino, F.T., G.P., S. Cocozza, M.P.**

Disclosures of conflicts of interest: **M. Tranfa** No relevant relationships. **V.C.** No relevant relationships. **R.G.** No relevant relationships. **G.C.** No relevant relationships. **S. Capasso** No relevant relationships. **V.B.M.** Grants from Italian Multiple Sclerosis Federation and Roche; honoraria from Almirall, Biogen, Bristol-Myers Squibb Celgene, Janssen, Merck, Novartis, Roche, Sanofi-Genzyme, Bayer, Mylan, Teva, and Viatris. **A. Carotenuto** Grants from Almirall and MAGNIMS-ECTRIMS; payment or honoraria for lectures, presentations, speakers bureaus, manuscript writing, or education events from Roche, Novartis, Sanofi, Merck, Almirall, Alexion, Bristol-Myers Squibb, and Biogen; support for attending meetings and/or travel from Roche, Novartis, Sanofi, Merck, Almirall, Alexion, Bristol-Myers Squibb, and Biogen. **A.C.** No relevant relationships. **R.L.** Consulting fees from Merck, Biogen, Novartis, Sanofi, Roche, Alexion, and Amgen; payment or honoraria for lectures, presentations, speakers bureaus, manuscript writing, or educational events from Merck, Biogen, Novartis, Sanofi, Roche, Alexion, and Amgen; payment for expert testimony from Merck, Biogen, Novartis, Sanofi, Roche, Alexion, and Amgen; support for attending meetings and/or travel from Merck, Biogen, Novartis, Sanofi, Roche, Alexion, and Amgen; medical writing support from Merck. **M.M.** Grants to institution from the Ministry of University and Research PNRR Extended Partnership (MNESYS no. PE00000006 and Digital Health Solutions in Community Medicine no. PNC-E3-2022-23683267); Campania Region Research Fund (NEURODIATE no. E65E24002260002); payment from AbbVie, Biogen, Bristol-Myers Squibb Celgene, Ipsen, Janssen, Merck, Novartis, Roche, and Sanofi-Genzyme. **A.S.** No relevant relationships. **M. Tarantino** No relevant relationships. **F.T.** No relevant relationships. **G.P.** No relevant relationships. **S. Cocozza** Research grants from FISM and Telethon; consulting fees from TTLC; fees for advisory board from Amicus Therapeutics. **M.P.** Payments made to institution from Baroni Foundation, Italian Ministry of University and Research, Fondazione Italiana Sclerosi Multipla; consulting fees from Biogen; payments from HEALTH&LIFE, AIM Education, Biogen, Novartis and FARECOMUNICAZIONE; payment for participation on a DataSafety monitoring board or advisory board from Biogen.

References

1. Walton C, King R, Rechtman L, et al. Rising prevalence of multiple sclerosis worldwide: Insights from the Atlas of MS, third edition. Mult Scler 2020;26(14):1816–1821.
2. Bebo B, Cintina I, LaRocca N, et al. The Economic Burden of Multiple Sclerosis in the United States: Estimate of Direct and Indirect Costs. Neurology 2022;98(18):e1810–e1817.
3. Battaglia MA, Bezzini D, Cecchini I, et al. Patients with multiple sclerosis: a burden and cost of illness study. J Neurol 2022;269(9):5127–5135.
4. Filippi M, Preziosa P, Arnold DL, et al. Present and future of the diagnostic work-up of multiple sclerosis: the imaging perspective. J Neurol 2023;270(3):1286–1299.

5. Rjeily NB, Solomon AJ. Misdiagnosis of Multiple Sclerosis: Past, Present, and Future. Curr Neurol Neurosci Rep 2024;24(11):547–557. [Published correction appears in Curr Neurol Neurosci Rep 2024;24(11):559.]
6. Montalban X. Revisions of the McDonald Criteria. ECTRIMS Congress; Copenhagen, Denmark. Scientific Session 1: New diagnostic criteria; September 18-20, 2024. https://www.neurologylive.com/view/advancing-ms-diagnosis-2024-criteria-revision-xavier-montalban.
7. Meaton I, Altokhis A, Allen CM, et al. Paramagnetic rims are a promising diagnostic imaging biomarker in multiple sclerosis. Mult Scler 2022;28(14):2212–2220.
8. Absinta M, Sati P, Schindler M, et al. Persistent 7-tesla phase rim predicts poor outcome in new multiple sclerosis patient lesions. J Clin Invest 2016;126(7):2597–2609.
9. Absinta M, Sati P, Masuzzo F, et al. Association of Chronic Active Multiple Sclerosis Lesions With Disability In Vivo. JAMA Neurol 2019;76(12):1474–1483. [Published correction appears in JAMA Neurol 2019;76(12):1520.]
10. Dal-Bianco A, Grabner G, Kronnerwetter C, et al. Slow expansion of multiple sclerosis iron rim lesions: pathology and 7 T magnetic resonance imaging. Acta Neuropathol 2017;133(1):25–42.
11. Dal-Bianco A, Grabner G, Kronnerwetter C, et al. Long-term evolution of multiple sclerosis iron rim lesions in 7 T MRI. Brain 2021;144(3):833–847.
12. Sati P, Thomasson DM, Li N, et al. Rapid, high-resolution, whole-brain, susceptibility-based MRI of multiple sclerosis. Mult Scler 2014;20(11):1464–1470.
13. Wuerfel J, Sinnecker T, Ringelstein EB, et al. Lesion morphology at 7 Tesla MRI differentiates Susac syndrome from multiple sclerosis. Mult Scler 2012;18(11):1592–1599.
14. Guo Z, Long L, Qiu W, et al. The Distributional Characteristics of Multiple Sclerosis Lesions on Quantitative Susceptibility Mapping and Their Correlation With Clinical Severity. Front Neurol 2021;12:647519.
15. Wittayer M, Weber CE, Platten M, Schirmer L, Gass A, Eisele P. Spatial distribution of multiple sclerosis iron rim lesions and their impact on disability. Mult Scler Relat Disord 2022;64:103967.
16. Cagol A, Benkert P, Melie-Garcia L, et al. Association of Spinal Cord Atrophy and Brain Paramagnetic Rim Lesions With Progression Independent of Relapse Activity in People With MS. Neurology 2024;102(1):e207768. [Published correction appears in Neurology 2024;103(1):e20959.]
17. La Rosa F, Wynen M, Al-Louzi O, et al. Cortical lesions, central vein sign, and paramagnetic rim lesions in multiple sclerosis: Emerging machine learning techniques and future avenues. Neuroimage Clin 2022;36:103205.
18. Ng Kee Kwong KC, Mollison D, Meijboom R, et al. The prevalence of paramagnetic rim lesions in multiple sclerosis: A systematic review and meta-analysis. PLoS ONE 2021;16(9):e0256845.
19. Moher D, Liberati A, Tetzlaff J, Altman DG; PRISMA Group. Preferred reporting items for systematic reviews and meta-analyses: the PRISMA statement. BMJ 2009;339:b2535.
20. Gillen KM, Nguyen TD, Dimov A, et al. Quantitative susceptibility mapping is more sensitive and specific than phase imaging in detecting chronic active multiple sclerosis lesion rims: pathological validation. Brain Commun 2025;7(1):fcaf011.
21. Munn Z, Moola S, Lisy K, Riitano D, Tufanaru C. Methodological guidance for systematic reviews of observational epidemiological studies reporting prevalence and cumulative incidence data. Int J Evid Based Healthc 2015;13(3):147–153.
22. Bagnato F, Sati P, Hemond CC, et al. Imaging chronic active lesions in multiple sclerosis: a consensus statement. Brain 2024;147(9):2913–2933.
23. Margoni M, Preziosa P, Storelli L, et al. Paramagnetic rim and core sign lesions in paediatric multiple sclerosis patients. J Neurol Neurosurg Psychiatry 2023;94(10):873–876.
24. Micheletti L, Maldonado FR, Watal P, et al. Utility of paramagnetic rim lesions on 1.5-T susceptibility phase imaging for the diagnosis of pediatric multiple sclerosis. Pediatr Radiol 2022;52(1):97–103.
25. Sacco S, Virupakshaiah A, Papinutto N, et al. Susceptibility-based imaging aids accurate distinction of pediatric-onset MS from myelin oligodendrocyte glycoprotein antibody-associated disease. Mult Scler 2023;29(14):1736–1747.
26. Treaba CA, Conti A, Klawiter EC, et al. Cortical and phase rim lesions on 7 T MRI as markers of multiple sclerosis disease progression. Brain Commun 2021;3(3):fcab134.
27. Lehto J, Nylund M, Matilainen M, et al. Longitudinal stability of progression-related microglial activity during teriflunomide treatment in patients with multiple sclerosis. Eur J Neurol 2023;30(8):2365–2375.
28. Lipka A, Bogner W, Dal-Bianco A, et al. Metabolic Insights into Iron Deposition in Relapsing-Remitting Multiple Sclerosis via 7 T Magnetic Resonance Spectroscopic Imaging. Neuroimage Clin 2023;40:103524.
29. Clark KA, Manning AR, Chen L, et al. Early Magnetic Resonance Imaging Features of New Paramagnetic Rim Lesions in Multiple Sclerosis. Ann Neurol 2023;94(4):736–744.
30. Yao Y, Nguyen TD, Pandya S, et al. Combining Quantitative Susceptibility Mapping with Automatic Zero Reference (QSM0) and Myelin Water Fraction Imaging to Quantify Iron-Related Myelin Damage in Chronic Active MS Lesions. AJNR Am J Neuroradiol 2018;39(2):303–310.
31. Jang J, Nam Y, Choi Y, et al. Paramagnetic Rims in Multiple Sclerosis and Neuromyelitis Optica Spectrum Disorder: A Quantitative Susceptibility Mapping Study with 3-T MRI. J Clin Neurol 2020;16(4):562–572.
32. Kuhlmann T, Moccia M, Coetzee T, et al; International Advisory Committee on Clinical Trials in Multiple Sclerosis. Multiple sclerosis progression: time for a new mechanism-driven framework. Lancet Neurol 2023;22(1):78–88.
33. Ciccarelli O, Barkhof F, Calabrese M, et al; as the MAGNIMS Study Group. Using the Progression Independent of Relapse Activity Framework to Unveil the Pathobiological Foundations of Multiple Sclerosis. Neurology 2024;103(1):e209444.
34. Eshaghi A, Young AL, Wijeratne PA, et al. Identifying multiple sclerosis subtypes using unsupervised machine learning and MRI data. Nat Commun 2021;12(1):2078. [Published correction appears in Nat Commun 2021;12(1):3169.]
35. Tranfa M, Pontillo G, Petracca M, et al. Quantitative MRI in Multiple Sclerosis: From Theory to Application. AJNR Am J Neuroradiol 2022;43(12):1688–1695.
36. Maggi P, Bulcke CV, Pedrini E, et al. B cell depletion therapy does not resolve chronic active multiple sclerosis lesions. eBioMedicine 2023;94:104701.
37. Clarke MA, Cheek R, Kazimuddin HF, et al. Paramagnetic rim lesions and the central vein sign: Characterizing multiple sclerosis imaging markers. J Neuroimaging 2024;34(1):86–94.
38. Absinta M, Sati P, Gaitán MI, et al. Seven-tesla phase imaging of acute multiple sclerosis lesions: A new window into the inflammatory process. Ann Neurol 2013;74(5):669–678.
39. Blindenbacher N, Brunner E, Asseyer S, et al. Evaluation of the 'ring sign' and the 'core sign' as a magnetic resonance imaging marker of disease activity and progression in clinically isolated syndrome and early multiple sclerosis. Mult Scler J Exp Transl Clin 2020;6(1):2055217320915480.
40. Barquero G, La Rosa F, Kebiri H, et al. RimNet: A deep 3D multimodal MRI architecture for paramagnetic rim lesion assessment in multiple sclerosis. Neuroimage Clin 2020;28:102412.
41. Lou C, Sati P, Absinta M, et al. Fully automated detection of paramagnetic rims in multiple sclerosis lesions on 3T susceptibility-based MR imaging. Neuroimage Clin 2021;32:102796.
42. Eisele P, Fischer K, Szabo K, Platten M, Gass A. Characterization of Contrast-Enhancing and Non-contrast-enhancing Multiple Sclerosis Lesions Using Susceptibility-Weighted Imaging. Front Neurol 2019;10:1082.
43. Altokhis AI, Hibbert AM, Allen CM, et al. Longitudinal clinical study of patients with iron rim lesions in multiple sclerosis. Mult Scler 2022;28(14):2202–2211.
44. Hemond CC, Reich DS, Dundamadappa SK. Paramagnetic Rim Lesions in Multiple Sclerosis: Comparison of Visualization at 1.5-T and 3-T MRI. AJR Am J Roentgenol 2022;219(1):120–131.
45. Barletta VT, Herranz E, Treaba CA, et al. In vivo characterization of microglia and myelin relation in multiple sclerosis by combined 11C-PBR28 PET and synthetic MRI. J Neurol 2023;270(6):3091–3102.
46. Calvi A, Clarke MA, Prados F, et al. Relationship between paramagnetic rim lesions and slowly expanding lesions in multiple sclerosis. Mult Scler 2023;29(3):352–362.
47. Chawla S, Kister I, Wuerfel J, et al. Iron and Non-Iron-Related Characteristics of Multiple Sclerosis and Neuromyelitis Optica Lesions at 7T MRI. Am J Neuroradiol 2016;37(7):1223–1230.
48. Coffman CH, White R, Subramanian K, Buch S, Bernitsas E, Haacke EM. Quantitative susceptibility mapping of both ring and non-ring white matter lesions in relapsing remitting multiple sclerosis. Magn Reson Imaging 2022;91:45–51.
49. Comabella M, Clarke MA, Schaedelin S, et al. CSF chitinase 3-like 1 is associated with iron rims in patients with a first demyelinating event. Mult Scler 2022;28(1):71–81.
50. Elliott C, Rudko DA, Arnold DL, et al. Lesion-level correspondence and longitudinal properties of paramagnetic rim and slowly expanding lesions in multiple sclerosis. Mult Scler 2023;29(6):680–690.
51. Haacke EM, Makki M, Ge Y, et al. Characterizing iron deposition in multiple sclerosis lesions using susceptibility weighted imaging. Magn Reson Imaging 2009;29(3):537–544.
52. Hagemeier J, Heininen-Brown M, Poloni GU, et al. Iron deposition in multiple sclerosis lesions measured by susceptibility-weighted imaging filtered phase: A case control study. Magn Reson Imaging 2012;36(1):73–83.
53. Hammond KE, Metcalf M, Carvajal L, et al. Quantitative in vivo magnetic resonance imaging of multiple sclerosis at 7 Tesla with sensitivity to iron. Ann Neurol 2008;64(6):707–713.
54. Hu H, Ye L, Ding S, et al. The heterogeneity of tissue destruction between iron rim lesions and non-iron rim lesions in multiple sclerosis: A diffusion MRI study. Mult Scler Relat Disord 2022;66:104070.
55. Huang W, Sweeney EM, Kaunzner UW, Wang Y, Gauthier SA, Nguyen TD. Quantitative susceptibility mapping versus phase imaging to

identify multiple sclerosis iron rim lesions with demyelination. J Neuroimaging 2022;32(4):667–675.
56. Kaunzner UW, Kang Y, Zhang S, et al. Quantitative susceptibility mapping identifies inflammation in a subset of chronic multiple sclerosis lesions. Brain 2019;142(1):133–145.
57. Kilsdonk ID, Lopez-Soriano A, Kuijer JPA, et al. Morphological features of MS lesions on FLAIR* at 7 T and their relation to patient characteristics. J Neurol 2014;261(7):1356–1364.
58. Kim S, Lee EK, Song CJ, Sohn E. Iron Rim Lesions as a Specific and Prognostic Biomarker of Multiple Sclerosis: 3T-Based Susceptibility-Weighted Imaging. Diagnostics. 2023;13(11):1866.
59. Kollia K, Maderwald S, Putzki N, et al. First Clinical Study on Ultra-High-Field MR Imaging in Patients with Multiple Sclerosis: Comparison of 1.5T and 7T. AJNR Am J Neuroradiol 2009;30(4):699–702.
60. Krajnc N, Dal-Bianco A, Leutmezer F, et al. Association of paramagnetic rim lesions and retinal layer thickness in patients with multiple sclerosis. Mult Scler 2023;29(3):374–384.
61. Kwong KCN, Mollison D, Meijboom R, et al. Rim lesions are demonstrated in early relapsing–remitting multiple sclerosis using 3 T-based susceptibility-weighted imaging in a multi-institutional setting. Neuroradiology 2022;64(1):109–117.
62. Maggi P, Sati P, Nair G, et al. Paramagnetic Rim Lesions are Specific to Multiple Sclerosis: An International Multicenter 3T MRI Study. Ann Neurol 2020;88(5):1034–1042.
63. Maggi P, Kuhle J, Schädelin S, et al. Chronic White Matter Inflammation and Serum Neurofilament Levels in Multiple Sclerosis. Neurology 2021;97(6):e543–e553.
64. Naval-Baudin P, Pons-Escoda A, Camins À, et al. Deeply 3D-T1-TFE hypointense voxels are characteristic of phase-rim lesions in multiple sclerosis. Eur Radiol 2023;34(2):1337–1345.
65. Nylund M, Sucksdorff M, Matilainen M, Polvinen E, Tuisku J, Airas L. Phenotyping of multiple sclerosis lesions according to innate immune cell activation using 18 kDa translocator protein-PET. Brain Commun 2022;4(1):fcab301.
66. Oh J, Suthiphosuwan S, Sati P, et al. Cognitive impairment, the central vein sign, and paramagnetic rim lesions in RIS. Mult Scler 2021;27(14):2199–2208.
67. Pinto C, Cambron M, Dobai A, Vanheule E, Casselman JW. Smoldering lesions in MS: if you like it then you should put a rim on it. Neuroradiology. 2022;64(4):703–714.
68. Rahmanzadeh R, Galbusera R, Lu P, et al. A New Advanced MRI Biomarker for Remyelinated Lesions in Multiple Sclerosis. Ann Neurol 2022;92(3):486–502.
69. Reeves JA, Weinstock Z, Zivadinov R, et al. Paramagnetic rim lesions are associated with greater incidence of relapse and worse cognitive recovery following relapse. Mult Scler 2023;29(8):1033–1038.
70. Shi Z, Pan Y, Yan Z, et al. Microstructural alterations in different types of lesions and their perilesional white matter in relapsing-remitting multiple sclerosis based on diffusion kurtosis imaging. Mult Scler Relat Disord 2023;71:104572.
71. Sinnecker T, Dörr J, Pfueller CF, et al. Distinct lesion morphology at 7-T MRI differentiates neuromyelitis optica from multiple sclerosis. Neurology 2012;79(7):708–714.
72. Suzuki M, Kudo K, Sasaki M, et al. Detection of Active Plaques in Multiple Sclerosis using Susceptibility-weighted Imaging: Comparison with Gadolinium-enhanced MR Imaging. Magn Reson Med Sci 2011;10(3):185–192.
73. Tolaymat B, Zheng W, Chen H, Li X, Harrison DM. Sex-specific differences in rim appearance of multiple sclerosis lesions on quantitative susceptibility mapping. Mult Scler Relat Disord 2020;45:102317.
74. Tozlu C, Jamison K, Nguyen T, et al. Structural disconnectivity from paramagnetic rim lesions is related to disability in multiple sclerosis. Brain Behav 2021;11(10):e2353.
75. Vanheule E, Cambron M, Dobai A, Casselman JW. Rim lesions in MS at 3T: clinical correlation and possible radiological alternatives for daily practice at lower field strength. J Neuroradiol 2024;51(4):101165.
76. Wang X, Zhu Q, Yan Z, et al. Enlarged choroid plexus related to iron rim lesions and deep gray matter atrophy in relapsing-remitting multiple sclerosis. Mult Scler Relat Disord 2023;75:104740.
77. Weber CE, Krämer J, Wittayer M, et al. Association of iron rim lesions with brain and cervical cord volume in relapsing multiple sclerosis. Eur Radiol 2022;32(3):2012–2022.
78. Yao B, Bagnato F, Matsuura E, et al. Chronic Multiple Sclerosis Lesions: Characterization with High-Field-Strength MR Imaging. Radiology 2012;262(1):206–215.
79. Zhang S, Nguyen TD, Hurtado Rúa SM, et al. Quantitative Susceptibility Mapping of Time-Dependent Susceptibility Changes in Multiple Sclerosis Lesions. AJNR Am J Neuroradiol 2019;40(6):987–993.
80. Zhang H, Nguyen TD, Zhang J, et al. QSMRim-Net: Imbalance-aware learning for identification of chronic active multiple sclerosis lesions on quantitative susceptibility maps. Neuroimage Clin 2022;34:102979.